

ALMA Extends to 15-kilometre Baselines: Submillimetre Science down to 20-Milliarcsecond Resolution

Catherine Vlahakis^{1,2}
 Leonardo Testi²
 Paola Andreani^{2,3}

¹ Joint ALMA Observatory, Santiago, Chile

² ESO

³ ESO ALMA Regional Centre

From September to late November 2014, the Atacama Large Millimeter/submillimeter Array (ALMA) carried out a Long Baseline Campaign to test and verify baselines up to ~ 15 kilometres for the first time. The tests were successful, demonstrating the power of ALMA to produce submillimetre-wave imaging at resolutions of tens of milliarcseconds. Science Verification observations of five targets, including an asteroid, a protoplanetary disc, an evolved star and a gravitationally lensed high-redshift galaxy, were obtained. The results demonstrate that the scientific leap for which ALMA was planned has been made. A brief overview of the 2014 Long Baseline Campaign and its scientific results are presented.

ALMA is a global project with partners in Europe, North America (USA and Canada) and East Asia (Japan, Taiwan and the Republic of Korea), to build and

operate the world's largest millimetre/submillimetre array, located on the Chajnantor Plateau in the north of Chile at an elevation of 5000 metres above sea level. ALMA, inaugurated in 2013, has a full complement of 66 antennas. The Call for Proposals for Early Science Cycle 3 has recently closed, with a record number of proposals received.

A key new capability offered in Cycle 3 is observing at high angular resolution using baselines of up to ten kilometres. This mode was tested and verified during a dedicated campaign held in the last quarter of 2014. A summary of this campaign — the 2014 ALMA Long Baseline Campaign — is presented here. Activities continue to extend and upgrade the capabilities, including new receivers, digital electronics, data handling and analysis software, and new observing modes (such as millimetre-wave very long baseline interferometry), with the goal of maintaining ALMA at the forefront of astrophysical research for many decades to come.

The 2014 ALMA Long Baseline Campaign

Imaging at resolutions of tens of milliarcseconds (mas) is a major goal of ALMA. This requires baselines of up to almost 16 kilometres, achieved using the distant

antenna stations on the Chajnantor site that have been built for this purpose, stretching out to almost ten kilometres from the centre of the array. The 2014 ALMA Long Baseline Campaign (LBC) carried out the first ever tests using these distant antenna stations; it was the first time the whole observatory infrastructure had been used for antenna separations above about three kilometres. The LBC tests were carried out from September to November 2014 and consisted of extensive testing with 23 antennas on long baselines of up to 15 kilometres, together with additional antennas on short (about 300 metres) baselines in order to provide the short spacings that are necessary for imaging extended objects. A total of 22–36 antennas were employed for the LBC tests, with the number depending on observing band; most tests were carried out in Band 3 (100 GHz). A paper (ALMA Partnership, Fomalont et al., 2015; hereafter ALMA I) provides details of the technical and calibration aspects of the LBC, and a brief summary is given here.

ALMA calibration normally uses the phase referencing observing mode, whereby short scans of the science target and a nearby quasar calibrator target are alternated over the duration of the observation, such that the phase measured on the calibrator can be transferred to the target. The accuracy with which this can be

Clem & Adri Bacri-Normier (wingsforscience.com)/ESO



Figure 1. The ALMA Chajnantor site from the air in early 2013.

achieved was a critical factor for the outcome of the long baseline observations, and was addressed with a test strategy that included: a) establishing the phase coherence of the long baseline array by carrying out test observations of quasars; b) determining the observing strategy needed to achieve good imaging results; and c) carrying out Science Verification (SV) observations to demonstrate the end-to-end process from observation to calibration to imaging. In order to address the former two points, the LBC tests included:

- 1) determination of the statistics of the temporal phase variation as a function of baseline length using observations of a single bright quasar;
- 2) determination of the accuracy of the phase transfer using alternating observations of two quasars that are close together on the sky;
- 3) development of a quasi real-time method to estimate the feasibility of given long baseline observations;
- 4) determination of the optimal time interval (cycle time) between calibrator scans;
- 5) determination of antenna positions and delay model errors using observations of many quasars distributed over the sky;
- 6) flux density measurement for candidate weak phase calibrators;
- 7) investigation of potential significant structure in calibrator sources when observed at long baselines; and
- 8) measurement of the positional accuracy at long baselines, by phase referencing among many quasars that are close together on the sky.

Details of these experiments, the analysis and conclusions are described in ALMA I.

An enormous amount was learned about ALMA observing at long baselines during the highly successful LBC and some of the main results are briefly summarised here (see ALMA I for details). Further investigations are also ongoing, and additional long baseline testing will take place in the last quarter of 2015 in order to further improve the observing mode and test long baseline imaging at higher frequencies.

It was found that calibration via phase referencing should, for most sources, only be carried out when the short-

term phase root mean square (rms) is < 30 degrees. The cycle time needed for phase referencing calibration to produce good image quality was found to be 60–90 seconds in almost all cases. The most reliable method of determining whether phase conditions are suitable for carrying out a given observation of a science target is with short observations of a strong quasar (the “Go/noGo” procedure), rather than predictions. The water vapour radiometer (WVR) correction, which takes into account estimated variations in the amount of precipitable water vapour along the line of sight to each antenna (see Nikolic et al., 2011; 2013), typically improves the phase noise by a factor of about two for clear skies, and further phase fluctuations are thought to be due to variations in the dry atmosphere.

The lack of an accurate dry atmospheric delay model, due to pressure variation across the array over distances of several kilometres and the current single pressure measurement at the centre of the array, is the dominant cause of systematic phase differences (longer-term variations, i.e., over timescales of minutes to hours) between observations of the phase calibrator and the science target. The addition of further weather stations in the coming months, providing several pressure measurements across the array, will allow improvement of the delay model and will be the main focus of the further long baseline testing later in 2015. It is also expected that the addition of further pressure sensors will improve the astrometric accuracy.

The survey for weak calibrators will continue in order to increase the number of sources in the ALMA calibrator catalogue (Fomalont et al., 2014). However, in order to find the faintest usable calibrators, and thereby ensure that a suitable calibrator can be found close enough to a science target, it is likely that a different observing strategy may need to be adopted in future.

For some of the SV targets (see the next section for details), the emission was sufficiently strong that it was possible to use the self-calibration technique to improve the image quality. For Juno, self-calibration provided an improvement in

the peak/image rms of a factor of two to six compared to imaging with phase referencing alone. For HL Tau, the improvement was up to a factor of two. For SDP.81, self calibration was not possible at all. Conversely, for the quasar 3C 138, which has emission that is dominated by a strong compact core and other relatively simple structures, the improvement ranged from a factor of 15 to 30. See ALMA I for further details. Thus, more sophisticated methods of self calibration may need to be implemented in future for some extended sources. Another finding from the SV imaging was that in many cases the integration time on source may be driven not by the need to reach a given signal rms, but by the need to obtain sufficient coverage of the uv (Fourier domain) plane.

Science Verification observations at long baselines

Continuum and spectral line observations of five SV targets were carried out to demonstrate the long baseline potential of ALMA, chosen from a broad range of science topics. The targets were the asteroid Juno, the asymptotic giant branch (AGB) star Mira, the circumstellar disc around the young star HL Tau, the quasar 3C 138, and the gravitationally lensed submillimetre galaxy SDP.81. The baselines typically ranged from 15 metres to ~ 15 kilometres, and observations were taken in two or three bands (selected from Bands 3, 4, 6 and 7). The fully verified SV datasets are publicly available on the ALMA Science Portal¹.

The results of the LBC are presented in a collection of four ApJ Letters by the ALMA Partnership. A summary of the main test results and SV observations is presented in ALMA I. Initial results on the SV targets Juno, HL Tau and SDP.81 are presented in ALMA Partnership, Hunter et al. (2015; hereafter ALMA II), ALMA Partnership, Brogan et al. (2015; hereafter ALMA III) and ALMA Partnership, Vlahakis et al. (2015; hereafter ALMA IV), respectively.

Juno

ALMA’s combination of excellent continuum brightness sensitivity at high angular resolution and well-matched wavelength

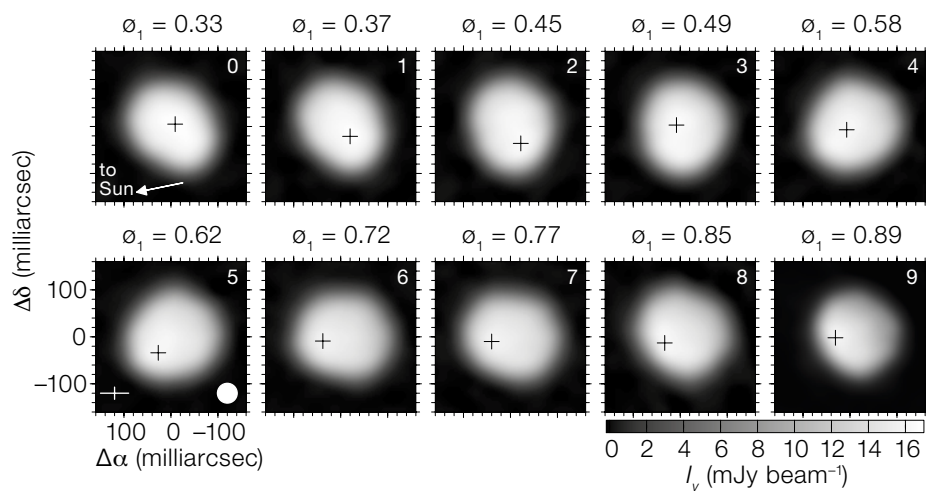


Figure 2. The sequence of ten ALMA LBC 1.3 millimetre continuum images of asteroid 3 Juno obtained over 60% of a 7.2-hour rotation, labelled by the rotation phase. The cross marks the position of peak intensity. From ALMA Partnership, Hunter et al. (2015).

coverage will enable mapping of the shape and surface temperature distribution for large numbers of main belt asteroids and Jupiter Trojans when using the full high angular resolution capability. With physical temperatures of 100–200 K, it should be possible to image these types of bodies at high signal-to-noise (S/N) at resolutions as fine as ~10 kilometres. The LBC SV observations of the asteroid 3 Juno, obtained in October 2014 in five blocks covering four hours, provided the first ground-based images to significantly resolve the surface of an asteroid at millimetre wavelengths (1.3 mm, 233 GHz). Full details can be found in ALMA II.

Juno is a member of the S-class of asteroids (stony composite of metallic iron and iron-bearing silicates). Its apparent mean diameter (from occultation studies) is 267 kilometres, although it is a triaxial ellipsoid and its rotation period is 7.21 hours. Its mean orbital radius is

2.67 astronomical units (au) and during the SV observations the illumination was 94%. Figure 2 shows the resulting ten 1.3-millimetre continuum images (two per observing block; labelled by rotational phase). The peak brightness temperature varies from 207 K to 222 K over the time sequence, with a median value of 215 K. Comparison with models of the size and shape of the asteroid from the Database of Asteroid Models from Inversion Techniques (DAMIT; Durech et al., 2010) shows good agreement (ALMA II).

While the LBC images of Juno provide a very good example of what ALMA can achieve for this asteroid at 233 GHz, observations of Juno and other main belt asteroids at shorter wavelengths would provide higher spatial resolution, e.g., ~20 kilometres at 345 GHz (Band 7) with a similar configuration when the asteroid is at a more favourable position (at a distance from Earth of ~1 au). ALMA

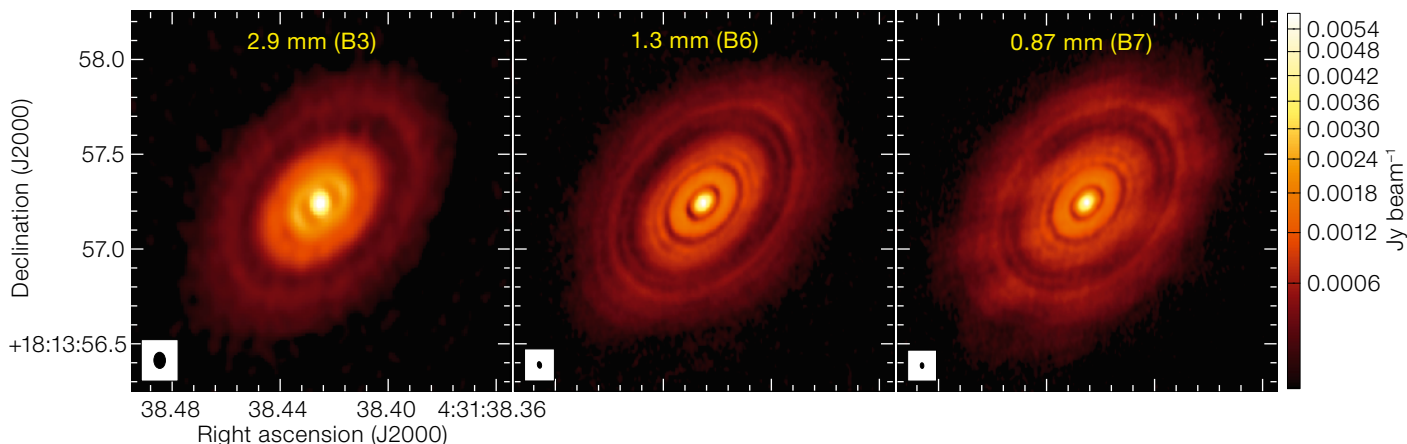
will also be able to provide improved long-term modelling of asteroid orbits, enabling improved prediction from the models, by delivering very accurate astrometry.

The HL Tau protoplanetary disc

The 1.3-millimetre ALMA image of HL Tau — a heavily embedded young stellar object surrounded by a protoplanetary disc — could be said to be synonymous with the success of the LBC, having been the first image to emerge from the early part of the campaign and the subject of a high-impact press release². The image was featured on the front cover of *Messenger* 158. However, the LBC SV for this source extended beyond this initial result, with data also observed at 2.9 mm (Band 3) and 0.87 mm (Band 7), achieving even higher angular resolution at 0.87 mm (25 mas, or 3.5 au at the distance of HL Tau).

HL Tau is located within a ~0.05 pc molecular ridge in the Taurus star-forming region, which is at a distance of 140 pc. While only observed as a conical reflection nebula at optical wavelengths, due to high extinction, HL Tau has however been well observed in the near- and mid-

Figure 3. ALMA continuum images of HL Tau at 102, 233 and 344 GHz (Bands 3, 6 and 7). The beam size is shown for each image. From ALMA Partnership, Brogan et al. (2015).



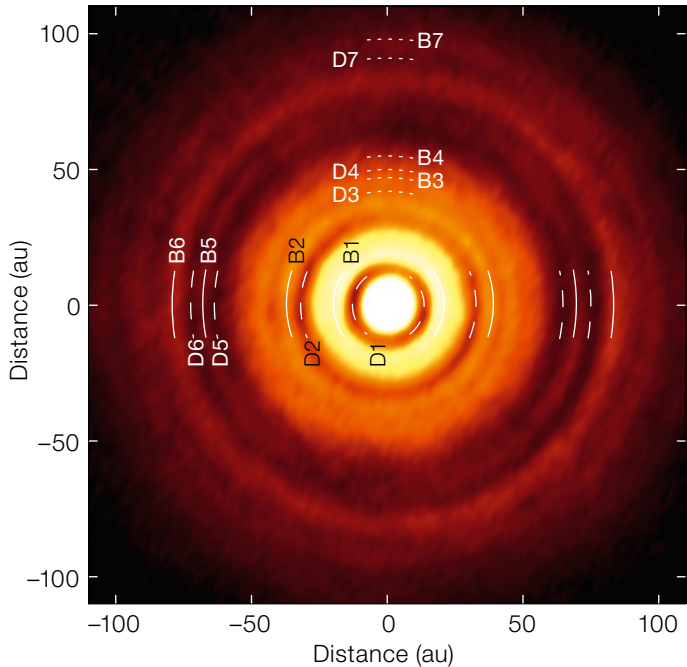


Figure 4. The deprojected 1.0 mm (287 GHz) ALMA image of the circumstellar disc around HL Tau at an angular resolution of 39×19 mas. From ALMA Partnership, Brogan et al. (2015).

$\text{HCO}^+(1-0)$, HCN, $^{12}\text{CO}(1-0)$ and CN. At this resolution the HL Tau region has complex outflow emission (see ALMA III). The $\text{HCO}^+(1-0)$ emission was also imaged at 0.25-arcsecond resolution: most of the outflow emission is resolved out, allowing the morphology of the HL Tau molecular gas disc to be spatially resolved for the first time (ALMA III).

The gravitationally lensed $z \sim 3$ submillimetre galaxy SDP.81

SDP.81 (HATLAS J090311.6+003906) is a $z = 3.042$ submillimetre galaxy gravitationally lensed by an intervening elliptical galaxy at $z = 0.299$. SDP.81 was first detected in the *Herschel* ATLAS (H-ATLAS) survey (Negrello et al., 2010) and subsequently resolved in the millimetre continuum as well as CO and H_2O molecular line emission at 0.6–3-arcsecond resolution with the Submillimeter Array (SMA) and the Plateau de Bure Interferometer (PdBI); see Bussmann et al. (2013) and Omont et al. (2013). As part of SV for the ALMA LBC, the target was observed in Bands 4, 6 and 7: Band 4 included the CO J=5-4 line, Band 6 the CO J=8-7 and the low excitation water line $\text{H}_2\text{O}(2_{02} - 1_{11})$ and Band 7 included the CO J=10-9 line. Full details are presented in ALMA IV.

Figure 5 shows the high resolution continuum images at Bands 4, 6 and 7, reaching angular resolutions as fine as 23 mas. This resolution is better than the Hubble Space Telescope images of this source, and corresponds to an unlensed spatial scale of ~ 180 pc in the lensed galaxy, or a few tens of pc in the source plane considering a magnification factor of ~ 11 –20. Viewed at this level of detail, strong detections of thermal dust emission in two incredibly thin arcs, which are the main components of an Einstein ring, were achieved. In addition to the eastern and western arcs, a continuum source was detected in all three bands at the central position of the lens (the early-type galaxy SDSS J090311.57+003906.5). This central continuum source is likely due to a weak, previously undetected, active galactic nucleus (AGN) in the foreground elliptical galaxy (see ALMA IV) and there is no evidence of a central lensed image in the molecular line data (Wong et al., 2015).

infrared; it is found to be a Class I–II protostar of spectral type around K5 with a collimated outflow. Since the HL Tau disc is one of the brightest at millimetre and submillimetre wavelengths, it has been a well-studied source since the early 1990s. The highest resolution observations prior to the ALMA LBC were obtained with the Combined Array for Research in Millimeter-wave Astronomy (CARMA) at a resolution of 0.13 arcseconds (18 au at 140 pc), which was sufficient to resolve the disc (Kwon et al., 2011).

ALMA observed HL Tau as part of the LBC in October–November 2014, using Bands 3, 6 and 7 (2.9, 1.3 and 0.87 mm, or ~ 100 , 240 and 345 GHz, respectively); details of the observations and initial analysis are presented in ALMA III. Figure 3 shows the continuum images; the size of the synthesised beam for the 0.87 mm Band 7 image is an impressive 30×19 mas. Figure 4 shows the combined Band 6 and 7 (1.0 mm) image, deprojected by the line of sight inclination of the disc of 46.72 degrees (derived from fitting each ring assuming circular orbits) with the bright and dark rings labelled (as B1–7 and D1–6, respectively). The spectral index (derived from the flux variation with wavelength across the three bands) is found to vary as a function of radial distance, with the dark rings having

a higher spectral index compared to the bright rings; rather than being entirely devoid of emission, the dark rings are likely to be optically thin. The centres of most of the rings are also found to be offset from the emission peak, making the rings non-circular, with HL Tau at one focus; the size of the offsets increases with the ring radius. Furthermore, there are apparent resonances between the radii of some of the rings.

The striking conclusion from ALMA III is that all these pieces of evidence, taken together, are highly suggestive of planet formation within the disc. Alternative interpretations have been discussed in the literature and involve grain growth promotion and trapping at specific locations in the disc, either due to instabilities or chemical/phase transitions in the gaseous component of the disc (Zhang et al., 2015). Further modelling and observations will elucidate the initial results from the LBC. The combination of high angular resolution and high fidelity imaging has already revealed a wealth of detail in the circumstellar disc, demonstrating the power of ALMA to deliver transformational science.

The HL Tau SV observations did not just include continuum emission. Four spectral lines were also imaged in Band 3, at 1.1-arcsecond angular resolution (~ 25 au):

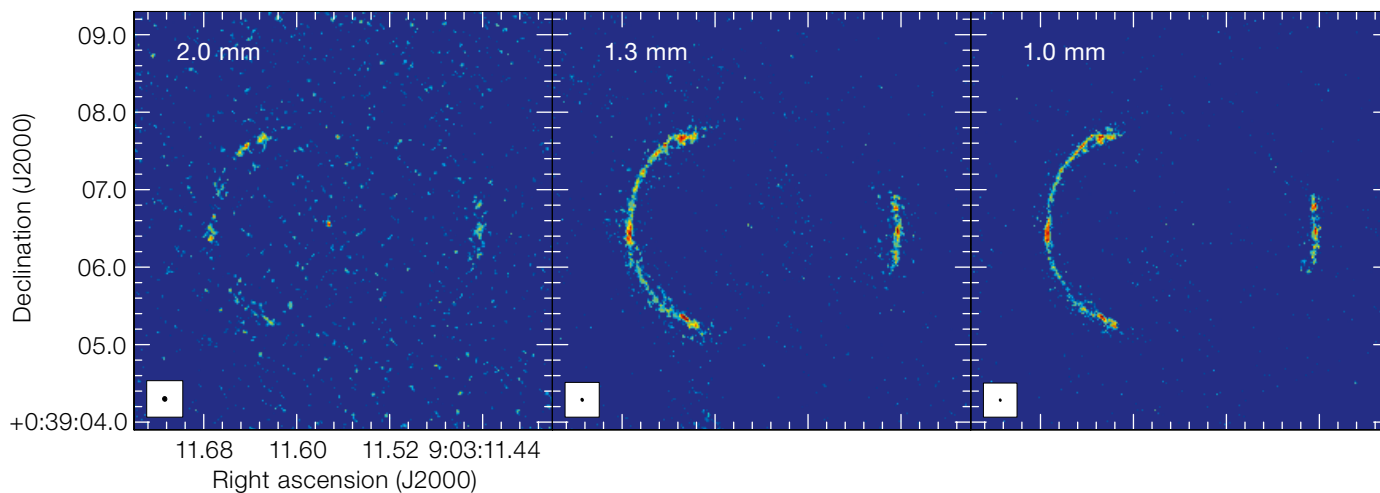
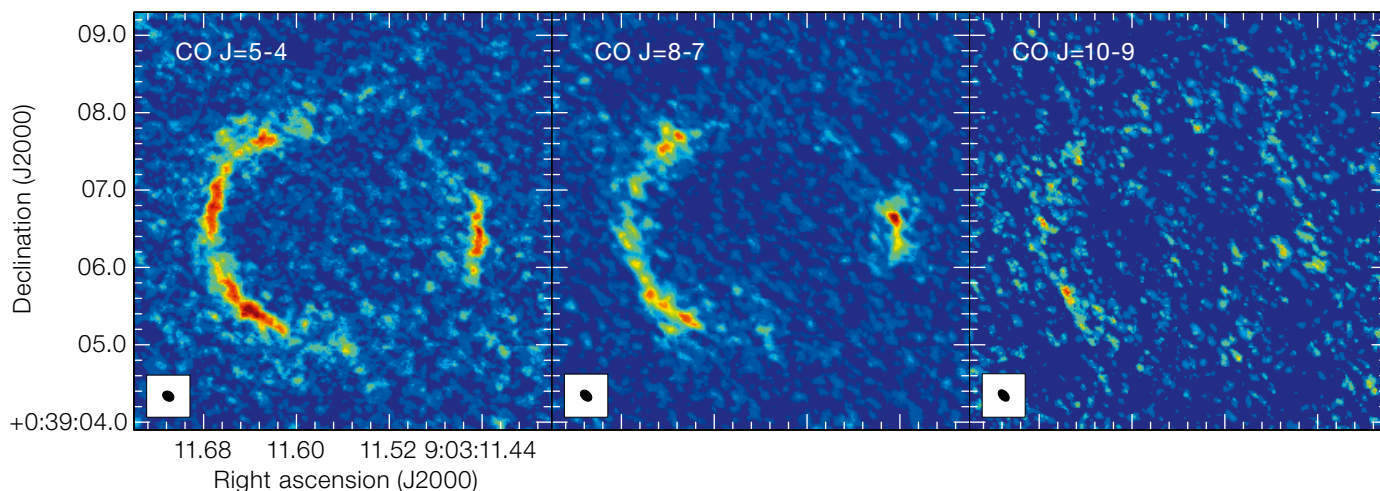


Figure 5. (Above) ALMA continuum images of the gravitationally lensed $z \sim 3$ galaxy SDP.81 in Bands 4 (2.0 mm), 6 (1.3 mm) and 7 (1.0 mm), left to right. The highest angular resolution, at 1.0 mm (290 GHz) in Band 7, is 31×23 mas (right panel). From ALMA Partnership, Vlahakis et al. (2015).

Figure 6. (Below) ALMA CO integrated intensity images of the gravitationally lensed $z \sim 3$ galaxy SDP.81 in Band 4 (CO J=5-4), Band 6 (CO J=8-7) and Band 7 (CO J=10-9), from left to right. The angular resolution is ~ 170 mas. From ALMA Partnership, Vlahakis et al. (2015).



The three transitions of CO (J=5-4, J=8-7 and J=10-8) were also imaged (see Figure 6). In order to achieve good S/N, the spectral lines were imaged at somewhat coarser resolution (~ 170 mas). The CO morphology is broadly similar to that seen in the continuum, tracing two main gravitational arcs; the CO emission in each arc, however, is clumpier. The spatially integrated CO line profiles show evidence of two components separated by ~ 300 km s $^{-1}$, with the lower velocity emission occurring predominantly in the western arc. Thermal H $_2$ O line emission was clearly detected in the eastern arc and at low S/N in the western arc, but to achieve these detections only the shorter

baselines were used, giving an angular resolution of ~ 0.9 arcseconds (ALMA IV). Nonetheless, with this detection at 0.9-arcsecond resolution, ALMA has achieved the highest resolution detection of thermal water emission in an extragalactic source to date. The water emission is confined to only one of the velocity components, in agreement with previous observations with the PdBI (Omont et al., 2013).

There have already been several additional studies based on the ALMA LBC observations, including one on mass modelling of the lensing elliptical at $z = 0.299$ that suggests a stellar core of

mass-to-light ratio of $\sim 2 M_{\odot} L_{\odot}^{-1}$, or a $> 3 \times 10^8 M_{\odot}$ black hole if an AGN is present (Tamura et al., 2015; Wong et al. 2015). Dye et al. (2015), Rybak et al. (2015a) and Swinbank et al. (2015) have modelled the background starburst galaxy and find a highly non-uniform distribution of dust clumps. Swinbank et al. (2015), for example, find a relatively smooth CO velocity field resembling disc-like dynamics and infer a rotating disc with a rotation velocity of 320 km s $^{-1}$; they suggest a disc that is in a state of collapse, and, from comparison with HST, the data suggest a scenario where two separate systems are merging. Alternative conclusions have been presented by

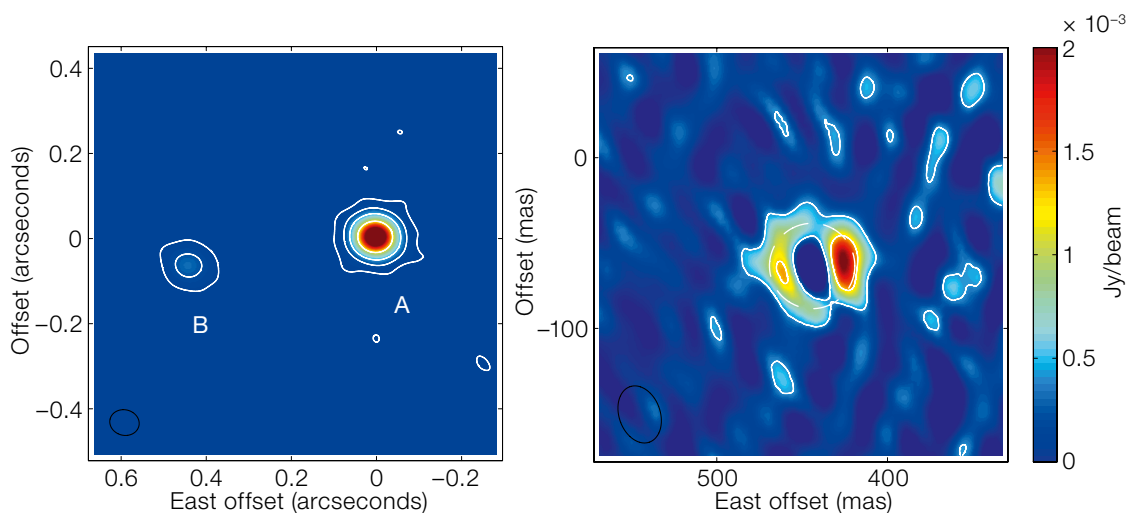


Figure 7. ALMA Band 3 image of Mira AB showing the binary (left) and the Band 6 image of Mira B with the point source subtracted, showing the partially ionised circumstellar shell (right). From Vlemmings et al. (2015).

other authors (Rybak et al., 2015b), and further analysis of the rich datasets will undoubtedly shed further light on the nature of this intriguing system.

The evolved star Mira

The archetypal long-period variable star Mira A (o Ceti) was observed in continuum and several spectral lines in Bands 3 and 6 as part of the LBC SV. Mira A, a mass-losing AGB star, is the primary in a binary system with a companion, Mira B (VZ Ceti; thought to be a white dwarf). At a distance of 92 pc (van Leeuwen, 2007), it is the closest such binary. The Mira AB system has already been observed in the CO J=3-2 line with ALMA in Cycle 1 (Ramstedt et al., 2014) and showed indications of a complex circumstellar envelope, but the binary pair was only marginally resolved. The LBC observations have an angular resolution as fine as ~ 25 mas and thus easily resolve the binary pair (see Figure 7).

Vlemmings et al. (2015) presented an analysis of the LBC SV continuum data, determining the size, shape, flux density and spectral index of both sources in the AB system. For the first time in the sub-millimetre, the extended atmosphere of a star was resolved — Mira A was resolved into an elliptical disc with a major axis of 42 mas (~ 3.8 au) at 94 GHz (Band 3) and 43 mas (4.0 au) at 229 GHz (Band 6). Brightness temperatures were found to be ~ 5300 K and 2500 K, respectively in

Bands 3 and 6, with a hotspot of $\sim 10\,000$ K brightness temperature on the stellar disc; it is suggested that the hotspot may be related to magnetic activity. A partially ionised region of ~ 2.4 au diameter (26 mas) around Mira B was also resolved (Figure 7, right), and the emission is found to be consistent with material close to the Mira B accretion disc that has been gravitationally captured from the AGB wind (see Vlemmings et al. [2015] for details).

Prospects

The ALMA LBC observations have been spectacularly successful, both in terms of reaching the high angular resolutions possible at these baselines and addressing potential atmospheric and instrumental limitations, and in terms of the quality and scientific value of the SV observations. A number of analyses have already been published based on the SV observations and more can be expected given the quality and scientific novelty of these data. As a result of the success of the LBC, the Call for Proposals for Cycle 3 included allocations for long baselines, up to ten kilometres for Bands 3, 4 and 6, and showed a very strong demand. A wealth of further exciting science can certainly be expected in the years to come as ALMA achieves its full potential for observing at very high resolution.

References

- ALMA Partnership, Brogan, C. L. et al. 2015, *ApJL*, arXiv:1503.02649 (ALMA III)
- ALMA Partnership, Fomalont, E. B. et al. 2015, *ApJL*, arXiv:1504.04877 (ALMA I)
- ALMA Partnership, Hunter, T. R. et al. 2015, *ApJL*, arXiv:1503.02650 (ALMA II)
- ALMA Partnership, Vlahakis, C. et al. 2015, *ApJL*, arXiv:1503.02652 (ALMA IV)
- Durech, J. et al. 2011, *Icarus*, 117, 313
- Dye, S. et al. 2015, *MNRAS*, submitted, arXiv:1503.08720
- Fomalont, E. et al. 2014, *The Messenger*, 155, 19
- Kwon, W. et al. 2011, *ApJ*, 741, 3
- Negrello, M. et al. 2010, *Science*, 440, 1999
- Nikolic, B. et al. 2011, *The Messenger*, 143, 11
- Nikolic, B. et al. 2013, *A&A*, 552, A104
- Omont, A. et al. 2013, *A&A*, 551, A115
- Ramstedt, S. et al. 2014, *A&A*, 570, L14
- Rybak, M. et al. 2015a, *MNRAS*, in press, arXiv:1503.02025
- Rybak, M. et al. 2015b, *MNRAS*, submitted, arXiv:1506.01425
- Swinbank, M. et al. 2015, *ApJL*, in press, arXiv:1505.05148
- Tamura, Y. et al. 2015, *PASJ*, in press, arXiv:1503.07605
- van Leeuwen, F. 2007, *A&A*, 474, 653
- Vlemmings, W. H. T. et al. 2015, *A&A*, 577, 4
- Wong, K. C. 2015, *ApJL*, submitted, arXiv:1503.05558
- Zhang, K., Blake, G. A. & Bergin, E. A. 2015, arXiv:1505.00882

Links

- ¹ ALMA Science Archive LBC data: <https://almascience.eso.org/news/release-of-science-verification-data-from-the-alma-long-baseline-campaign-2>
- ² LBC HL Tau Release: <http://www.eso.org/public/news/eso1436/>



FORS2 colour image of part of the shell of the large Galactic planetary nebula Abell 21 (Sharpless 2-274). Broadband images in *B*, *V*, *R* and narrow band images in the emission lines of [O III] 5007 Å and H α were combined. A21 is classified as a Type I planetary nebula, typically displaying enhanced He and N abundances, derived from a higher mass progenitor star. See Release eso1520 for details.

Probing the Effects of Stellar Evolution: The Dust and Gas in Detached Shells around AGB Stars

Matthias Maercker¹
Sofia Ramstedt²
Marcelo L. Leal-Ferreira³
Göran Olofsson⁴
Hans-Gustav Floren⁴

¹ Onsala Space Observatory, Dept. of Radio and Space Science, Chalmers University of Technology, Onsala, Sweden

² Department of Physics and Astronomy, Uppsala University, Sweden

³ Argelander Institut für Astronomie, University of Bonn, Germany

⁴ Department of Astronomy, Stockholm University, AlbaNova University Center, Sweden

In the last stages of their lives, Sun-like stars evolve along the asymptotic giant branch (AGB), and contribute a significant fraction of heavy elements to the interstellar medium, driving the chemical evolution of galaxies and providing the building material for new stars and planets. We observed the detached shells of dust around the evolved carbon AGB star R Scl in polarised, dust-scattered stellar light with the PolCor instrument on the ESO 3.6-metre telescope. The observations show the distribution of the dust in the shell with unprecedented detail. Comparison with high angular resolution observations of the molecular gas with ALMA show that dust and CO emission coincide almost exactly, implying a common evolution of the dust and gas since the creation of the shell. The results give unique insights into thermal pulses — the mechanism responsible for the chemical evolution of the star — and the way evolved stars lose their mass.

The thermally pulsing AGB

During its AGB evolution, a star periodically undergoes rapid helium burning in a shell around the core. This phenomenon is known as a thermal pulse (TP), and lasts for only a few hundred years every 10 000–100 000 years (Karakas & Lattanzio, 2007). The release of the extra energy into the stellar envelope causes the star to restructure, leading to the

formation of elements inside the star (mainly carbon and s-process elements). The new elements are mixed to the stellar surface and incorporated into the stellar wind, leading to the chemical evolution of the circumstellar envelope (CSE). In particular, the mixing of extra carbon leads to the evolution from oxygen-rich (or M-type) AGB stars (with an atmospheric abundance ratio $C/O < 1$) to carbon-rich AGB stars (with $C/O > 1$). Owing to their short duration, and the long time-scales between pulses, it is extremely unlikely that an AGB star will be observed during a TP directly. As a consequence, models of TPs have been essentially independent of observations (e.g., Karakas & Lattanzio, 2007).

The increase in mass-loss rate and wind velocity during a TP cycle leads to the creation of a shell that may sweep up previously ejected material, leading to the appearance of a detached shell (Steffen & Schönberner, 2000; Schöier et al., 2005; Mattsson et al., 2007). One of the few ways to study the TP phenomenon is from the observations of detached shells that

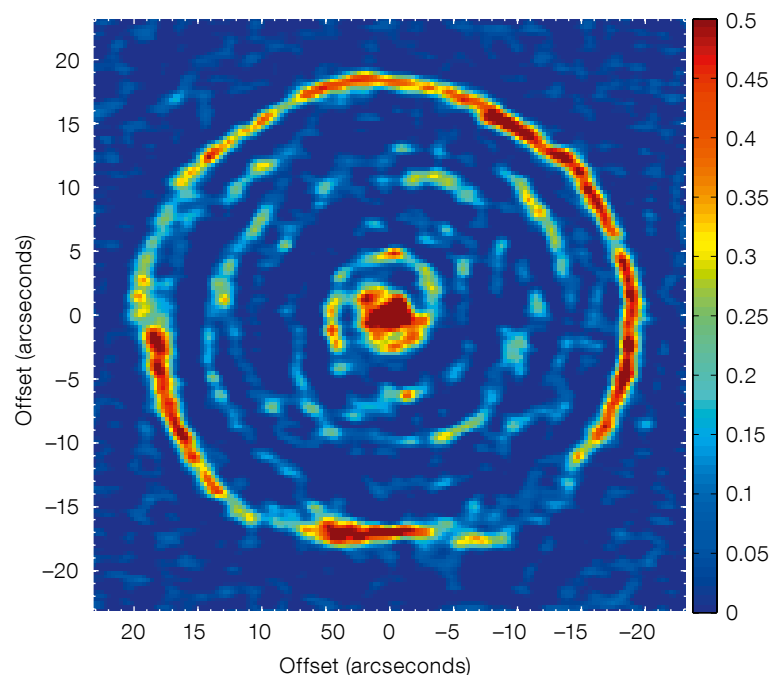
have been found around approximately ten carbon stars in molecular line emission, as well as in stellar dust-scattered light at optical wavelengths (e.g., Olofsson et al., 1996; 2010; Maercker et al., 2010; 2012; 2014).

Extensive studies in recent decades have shown the importance of AGB stars for the cosmic cycle of matter. However, central questions still remain to be answered. Although it is well established that these stars lose a large fraction of their mass in stellar winds, the wind-driving mechanism and geometry, and the molecular and dust content of the CSE, are not well known. In the prevailing theory, the stars lose their mass through radiation pressure on dust grains in the inner CSE. Collisions with the molecular gas drag the gas along, driving the mass loss. The interaction of the dust and gas is hence an integral part of the mass-loss mechanism. Detached shells offer a unique opportunity to study the evolution of the dust and gas and their role in the mass loss on the AGB.

The detached shell around R Sculptoris

The carbon AGB star R Scl is surrounded by a large (approx 20 arcseconds radius), geometrically thin (approximately 2 arc-

Figure 1. ALMA observations of the detached shell around R Scl in CO(3-2) emission. The image shows the detached shell and spiral structure at the stellar velocity. The colour scale is in Jy/beam (Maercker et al., 2012).



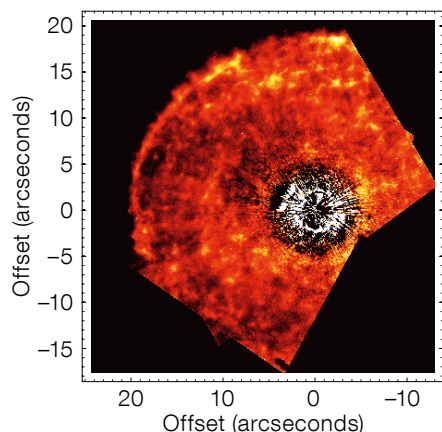


Figure 2. HST observations of the detached shell around R Scl in dust-scattered stellar light in the F814 filter observed with the Advanced Camera for Surveys (ACS) High Resolution Camera on HST. Due to the limited field of view of the ACS, only one third of the shell is covered in the image (from Olofsson et al., 2010).

seconds) shell of gas and dust. R Scl has been observed extensively with single-dish submillimetre observations (e.g., Olofsson et al., 1993). However, those low-resolution observations barely managed to resolve the shell of gas. High spatial resolution images of the detached gas shell in CO line emission were observed in the first cycle (Cycle 0) of

science observations with the Atacama Large Millimeter/submillimeter Array (ALMA; see Figure 1 and Maercker et al., 2012). The data clearly show the detached shell, as well as a binary-induced spiral structure extending from the shell, providing evidence of the present-day mass loss. Although overall spherically symmetric, the CO observations show a clearly clumpy structure, and deviations from a perfect sphere along the perimeter of the shell.

Observations of dust-scattered stellar light showed the detached dust shell at high spatial resolution using the EFOSC2 instrument on the ESO 3.6-metre telescope (González Delgado et al., 2001; 2003). A small-scale clumpy structure in the dust shell was revealed in fine images with the Hubble Space Telescope (HST) and is shown in Figure 2 (see Olofsson et al., 2010), albeit covering only approximately one third of the shell. The most complete observations of the dust shell were recently obtained with the PolCor instrument on the ESO 3.6-metre telescope. PolCor observed the CSE around R Scl in polarised, dust-scattered stellar light, imaging the entire detached shell in unprecedented detail (see Figure 3 and Maercker et al., 2014).

In addition to the detached shell around R Scl, the PolCor observations imaged the detached shell around the carbon AGB star V644 Sco (Figure 4). The shell around this star had been deduced from single-dish CO emission line observations, and estimated to have a radius of

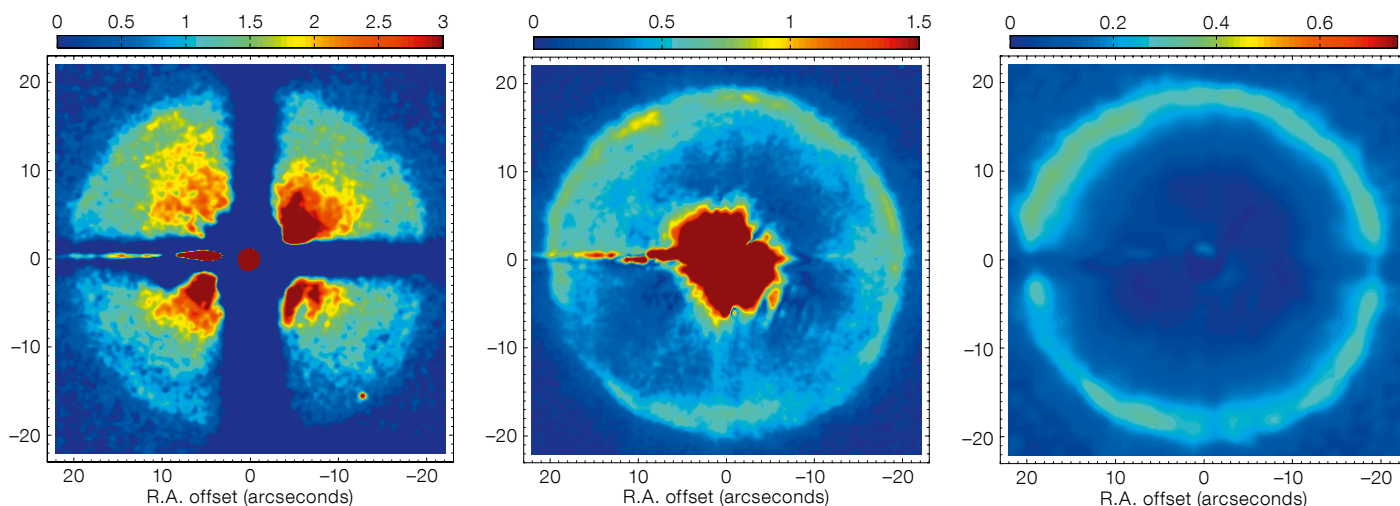
approximately 10 arcseconds. However, no direct image had ever been made before the PolCor observations, which, for the first time, directly constrain the size and width of the detached shell around V644 Sco.

PolCor and dust-scattered light

We imaged the detached shells around R Scl and V644 Sco in polarised, dust-scattered, stellar light using the PolCor instrument on the ESO 3.6-metre telescope. PolCor is a user instrument developed by the Department of Astronomy at Stockholm University (Ramstedt et al., 2011). It is a combined polariser and coronagraph, allowing the detection of faint, scattered light emission close to bright stars. A large number of short exposures allows the lucky imaging technique to be utilised, effectively resulting in high-quality images. The effective seeing in the observations of R Scl was typically reduced from 1.3 arcseconds during the observations to 0.9 arcseconds in the final shifted-and-added images. The pixel scale of the PolCor images was 0.114 arcseconds/pixel.

The images of the CSE of the detached shells were taken in V-band (0.55 μm) and R-band (0.64 μm). The light from the star is scattered by the dust grains in the CSE. The total amount of scattered light depends on the scattering efficiency and direction per grain, and on the total number of grains. The scattering efficiency mainly varies with grain size

Figure 3. PolCor observations of the CSE of R Scl in the R-band: total intensity (left), polarised intensity (middle), and degree of polarisation (right). The images are smoothed by a Gaussian kernel with a full width half maximum of two pixels (0.23 arcseconds). The total and polarised intensities are given in counts s^{-1} (from Maercker et al., 2014).



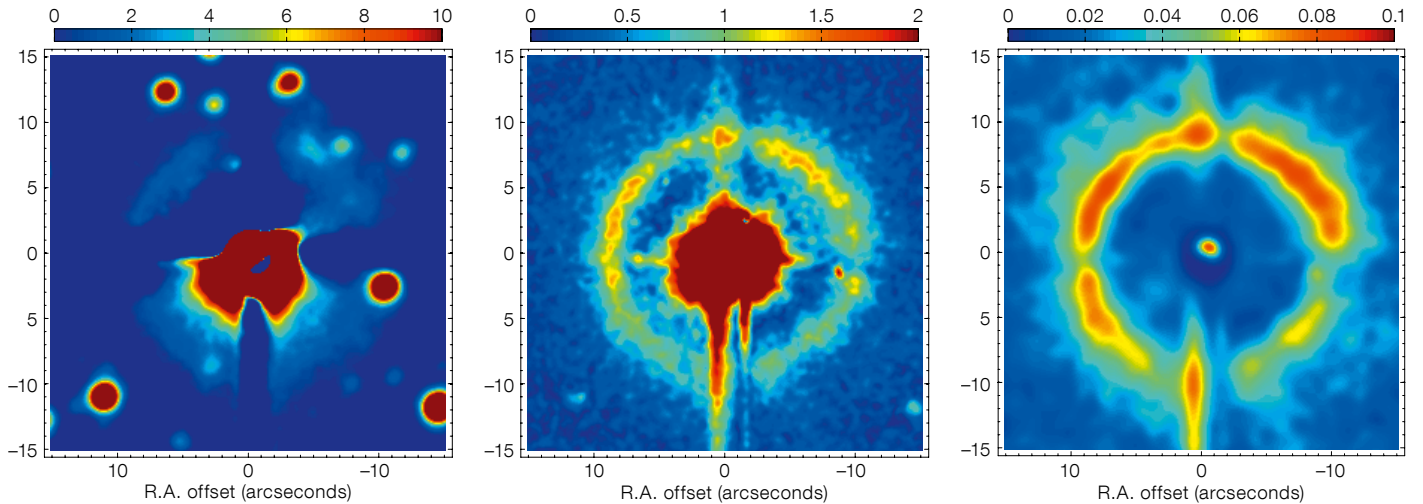


Figure 4. PolCor observations of the CSE of V644 Sco in the *R*-band: total intensity (left), polarised intensity (middle), and polarisation degree (right). The images are Gaussian smoothed (full width half

maximum 0.23 arcseconds) and the total and polarised intensities are in counts s^{-1} . The observations present the first direct images of the detached shell around V644 Sco (from Maercker et al., 2014).

(Olofsson et al., 2010) and observations of dust-scattered light effectively probe the distribution of dust grains in the CSE, independent of radiative transfer effects for low optical depths (as for thermal dust emission). Additionally, while the stellar light is essentially unpolarised, the scattering by the grains introduces a linear polarisation in scattered light. The degree of polarisation is highest when the angle between the incoming light and the direction of the scattered light is around 90 degrees. As a consequence, images of polarised, dust-scattered stellar light probe the distribution of the dust predominantly in the plane of the sky.

The PolCor observations were taken as part of a pilot project to test the instrument on the ESO 3.6-metre telescope and the feasibility of observing the dusty CSEs around AGB stars. A total of 14 evolved stars were observed, with varying stellar properties (e.g., mass-loss rates and binarity) and circumstellar morphologies. Due to their clearly extended nature and geometry, detached shell sources are readily analysed and interpreted by polarised light observations in the optical.

The detached dust shell with PolCor

The PolCor observations of the CSE around R Scl give the first complete view

of the detached dust shell around this star at high angular resolution. The shell is clearly detected in the total intensity and polarised images in both filters. Small-scale structure can also be seen along the shell in polarised light. The measured degree of polarisation is strongly affected by the subtraction of the stellar point spread function in the total intensity images (see Maercker et al. [2014] for details). We derive a lower limit for the degree of linear polarisation of 30%, indicating that a large amount of the dust mass is indeed confined to the shell.

The high image quality allows us to measure the radius and observed width of the shell to high accuracy, giving an average shell radius of 19.5 arcseconds and a width of 3.2 arcseconds. This measurement is confirmed by model profiles of stellar light scattered by dust particles in a homogeneous, thin, detached shell. The determined shell radius and width agrees well with previous estimates. However, the PolCor data is of such quality that it allows for direct comparison with the HST data for dust-scattered light (Figure 2). The Hubble field only covers part of the shell, but for the overlapping regions it is obvious that the PolCor data detects the same small-scale structure, indicative of a clumpy detached shell (Figure 5, upper). In contrast to the HST data however, the PolCor data shows

that the clumpy structure is not evenly distributed throughout the shell. In particular there appears to be less clumpy structure and limb brightening in the southwest quadrant of the shell.

Synergy between optical and submillimetre observations

The ALMA observations of R Scl provide the highest spatial resolution images of the detached shell in molecular gas to date. The resolution of the CO(3-2) observations in Band 7 is approx. 1.4 arcseconds (Maercker et al., 2012). It is hence possible to directly compare the distribution of the dust with the distribution of the gas in the detached shell. The ALMA observations at the stellar velocity and the polarised observations with PolCor both show the distribution of the gas and the dust in the plane of the sky, respectively (Figure 5, lower). The contours of the ALMA observations closely trace the emission seen in polarised intensity. In particular, the deviations from a perfect spherical shape are identical in both observations (most prominently the flattening of the shell in the south). The gas and dust hence have a nearly identical distribution, indicating that they have evolved together since the detached shell was created. This is in contrast to other detached shell sources, in particular the

carbon AGB star U Ant. Here a clear separation of the dust and gas was observed (Maercker et al., 2010). The shell around U Ant is about twice as old as the shell around R Scl. It is not clear whether the difference between the two objects is an evolutionary effect, or whether the dust and gas interaction differs.

The most detailed view of R Scl and thermal pulses

The PolCor images of R Scl give the most detailed view of the detached dust shell to date. Combined with the observations of the molecular gas with ALMA, this provides the strongest constraints on the thermal pulse cycle ever obtained observationally. The images of the dust-scattered light and CO line emission show a strong coupling between the dust and gas, constraining both the mass-loss mechanism during creation of the shell, as well as the interaction with a surrounding medium. The spiral shape observed in the ALMA data further constrains the evolution of the mass loss and expansion velocity since the shell was formed. Together this gives the most complete description of the thermal pulse cycle, and effectively constrains theoretical models observationally for the first time.

References

- González Delgado, D. et al. 2001, *A&A*, 372, 885
 González Delgado, D. et al. 2003, *A&A*, 399, 1021
 Karakas, A. & Lattanzio, J. C. 2007, *PASA*, 24, 103
 Maercker, M. et al. 2010, *A&A*, 511, A37
 Maercker, M. et al. 2012, *Nature*, 490, 232
 Maercker, M. et al. 2014, *A&A*, 570, A101
 Mattsson, L., Höfner, S. & Herwig, F. 2007, *A&A*, 470, 339
 Olofsson, H. et al. 1993, *ApJS*, 87, 267
 Ramstedt, S. et al. 2011, *A&A*, 531, A148
 Schöier, F. L., Lindqvist, M. & Olofsson, H. 2005, *A&A*, 436, 633

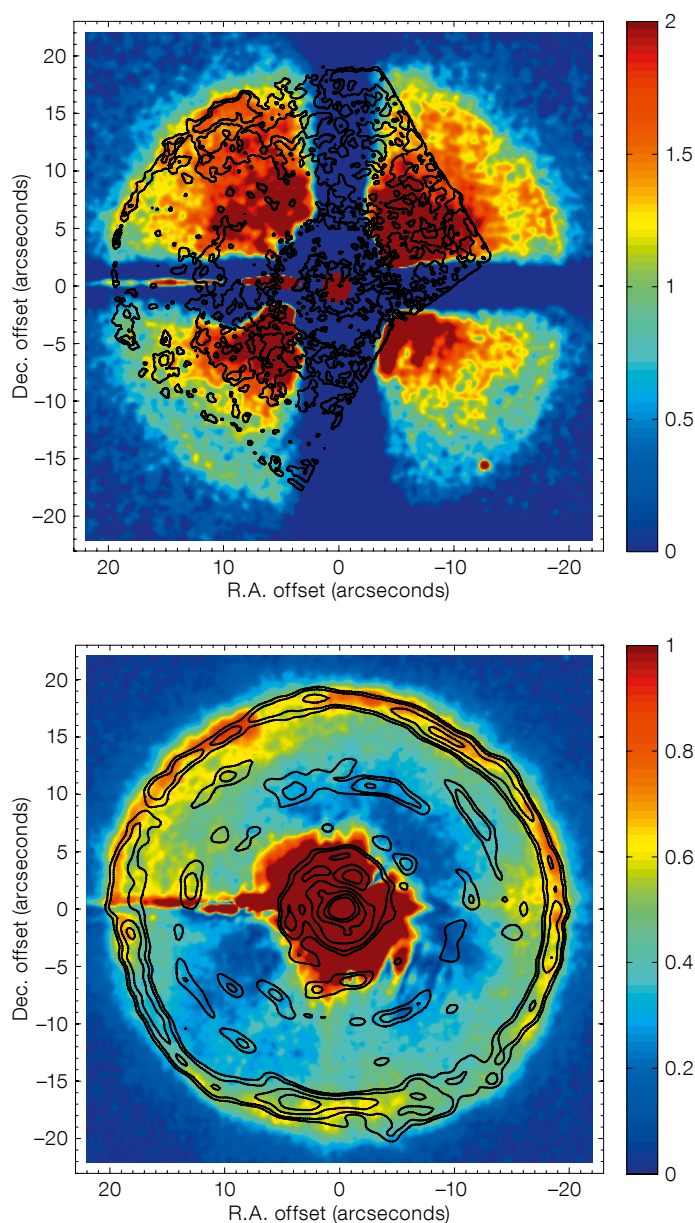


Figure 5. PolCor observations in *R*-band compared to HST and ALMA data. Top: PolCor total intensity image (colour) overlaid by the ACS F814 image (contours). Bottom: PolCor polarised intensity image (colour) overlaid by the ALMA CO(3-2) map at the stellar velocity, shown as contours (from Maercker et al., 2014).

OmegaWINGS: A VST Survey of Nearby Galaxy Clusters

Marco Gullieuszik¹
 Bianca Poggianti¹
 Giovanni Fasano¹
 Simone Zaggia¹
 Angela Paccagnella^{1,2}
 Alessia Moretti^{1,2}
 Daniela Bettoni¹
 Mauro D’Onofrio²
 Warrick J. Couch³
 Benedetta Vulcani⁴
 Jacopo Fritz⁵
 Alessandro Omizzolo^{1,6}
 Andrea Baruffolo¹
 Pietro Schipani⁷
 Massimo Capaccioli⁸
 Jesus Varela⁹

¹ INAF — Osservatorio astronomico di Padova, Italy

² Dipartimento di Fisica e Astronomia, Università degli Studi di Padova, Italy

³ Australian Astronomical Observatory, North Ryde, Australia

⁴ Kavli Institute for the Physics and Mathematics of the Universe (WPI), Todai Institutes for Advanced Study, The University of Tokyo, Kashiwa, Japan

⁵ Centro de Radioastronomía y Astrofísica, UNAM, Campus Morelia, Mexico

⁶ Specola Vaticana, Vatican City State

⁷ INAF — Osservatorio astronomico di Capodimonte, Napoli, Italy

⁸ Dipartimento di Fisica, Università Federico II, Napoli, Italy

⁹ Centro de Estudios de Física del Cosmos de Aragón, Teruel, Spain

OmegaWINGS is a photometric and spectroscopic survey of 46 nearby galaxy clusters. The photometric part is based on OmegaCAM imaging with the VLT Survey Telescope; the field of view of one square degree covers the whole virial region, extending up to the infall regions of each OmegaWINGS cluster. The ongoing spectroscopic survey will provide about 30 000 spectra with AAOmega on the Australian Astronomical Telescope. OmegaWINGS will provide an extremely detailed and complete view of galaxy populations in clusters. The final data products will include, for each galaxy detected in the target clusters, aperture and surface photometry, morphological type and a reliable characterisation of the stellar populations. The survey will therefore

be a unique tool to study the formation and evolution of galaxies in clusters and the interactions of galaxies with the environment.

The OmegaWINGS programme builds on the Wide-field Nearby Galaxy-cluster Survey (WINGS; Fasano et al., 2006) to carry out a photometric and spectroscopic campaign of nearby galaxy clusters ($0.04 < z < 0.07$). The WINGS survey is based on *B*- and *V*-band imaging for 76 clusters over a field of view of about 30 by 30 arcminutes carried out with the Wide Field Imager (WFI) on the MPG/ESO 2.2-metre telescope and the Wide Field Camera (WFC) on the Isaac Newton Telescope (INT). With the aim of covering the virial region and extending out into the infall region, we have obtained OmegaCAM Guaranteed Time Observations (GTO) imaging in the *u*-, *B*- and *V*-bands over 1 by 1 degree for 45 fields covering 46 WINGS clusters. The *u*-band campaign is ongoing, while the *B*- and *V*-band observations have been completed. With a median seeing of 1 arcsecond in both *B*- and *V*-bands, our 25-minute exposures in each band typically reach the 50% completeness level at $V = 23.1$ mag. Photometric catalogues are publicly available at the Centre de Données astronomiques de Strasbourg (CDS), and they will be included in the next release of the WINGS database at the Virtual Observatory, together with the OmegaCAM reduced images.

Galaxy clusters, the most massive collapsed structures in the Universe, play an important role for both cosmology and galaxy evolution studies. They are the tail of a continuum distribution of halo masses, and the most extreme environments where galaxy formation has proceeded at an accelerated rate compared to the rest of the Universe. Clusters have been a testbed for studies of galaxy formation and evolution, uncovering trends that several years later have also been found in the field. They are a repository for galaxies that have been shaped in lower halo-mass environments, but are also the sites where essentially all environmental effects are thought to take place, from strangulation to ram-pressure stripping, and even galaxy merging. As peaks in the matter distribution, galaxy clusters

host those galaxies that have formed first and in the most extreme primordial conditions. At the same time they are the sites where hierarchical growth is most evident, as in the case of the brightest cluster galaxies. There is no better place than rich clusters in the low-*z* Universe to find and study the descendants of the most massive galaxies observed at high-*z*.

The WINGS survey

The WINGS cluster survey sample consists of all clusters at redshift $0.04 < z < 0.07$ in both hemispheres at Galactic latitude $|b| > 20$ degrees selected from the ROSAT X-ray-Brightest Abell-type Cluster Sample, the Brightest Cluster Sample and its extension (Ebeling et al. [2000] and refs therein). For a subset of clusters, the original WINGS imaging in the *B*- and *V*-bands have been complemented with *J*- and *K*-band photometry obtained with the Wide Field Camera (WFCam) on the United Kingdom Infra-Red Telescope (UKIRT) and *u*-band photometry obtained with the INT, the Large Binocular Telescope and Bok telescopes. More than 6500 spectra were taken with the two-degree field instrument (2dF) on the AAT and Wide Field Fibre Optical Spectrograph (WYFFOS) on the William Herschel Telescope (WHT), both multi-fibre spectrographs.

These data allowed us to obtain aperture and surface photometry, the stellar mass and star formation history of the cluster galaxies, as well as to characterise the cluster substructure and dynamics. With these data we have conducted a number of studies on galaxy properties and evolution (a full publication list can be found at the WINGS website¹). The WINGS data and data products are publicly available through the Virtual Observatory, as explained in Moretti et al. (2014). The WINGS dataset is unique, for the quality and quantity of data on low-*z* clusters.

The main limitation of the original WINGS data is that they cover only the cluster cores: the maximum clustercentric distance reached in (almost) all clusters by the WINGS imaging is only 0.6 times the virial radius. Crucially, what is missing is the coverage out to at least the virial radius and into the outer regions. This is

of primary importance, as it links clusters with the surrounding populations and with the field. The outer regions of clusters are the transition regions between the core and the filaments and/or groups feeding the cluster, at the point where galaxies are subject to a dramatic change of environment. Indeed, observations have proved that the cluster outskirts are essential to the understanding of galaxy transformations. With the exception of a few single clusters and superclusters, this very important transition region between clusters and the surrounding field remains largely unexplored.

The OmegaWINGS survey

With the aim of covering the virial region and extending out into the infall region, we have obtained GTO OmegaCAM imaging in the u -, B - and V -bands over 1 by 1 degree for 45 fields covering 46 WINGS clusters. A large spectroscopic follow-up campaign targeting these clusters is ongoing with AAOmega on the AAT. We named this extension of the WINGS survey, OmegaWINGS.

OmegaWINGS targeted clusters were randomly selected from the 57 WINGS clusters that can be observed from the VST ($\delta < +20$ degrees). We obtained service mode B - and V -band imaging for 46 of them with 45 OmegaCAM pointings. The location of the target clusters observed by the OmegaWINGS survey is shown in Figure 1.

Observations started in October 2011, occurred through Periods 88, 89, 90, 91 and 93 and were concluded in September 2014. The total exposure time was 25 minutes for both B - and V -band observations. The seeing during the observations was lower than 1.3 and 1.2 arcseconds in 80% of B - and V -band images, respectively, with a median value of 1.0 arcseconds in both B - and V -band images. Figure 2 shows the final OmegaCAM V -band image of A2399. The projected radius (R_{200}) of the cluster and the field of view (FoV) of WINGS imaging obtained with the Wide-field Imager are shown for comparison. A complete description of the B - and V -band photometric surveys is presented in Gullieuszik et al. (2015).

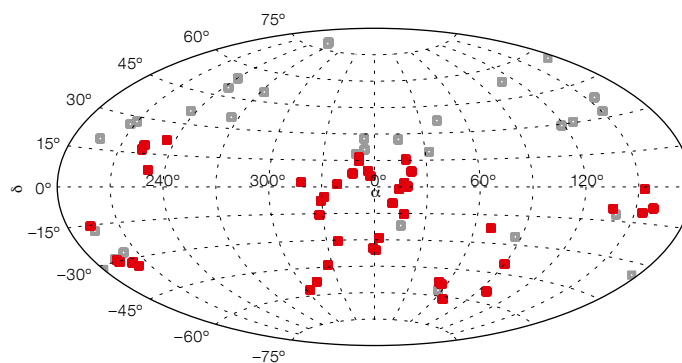


Figure 1. OmegaWINGS target clusters are shown as red squares; grey squares are all WINGS clusters.

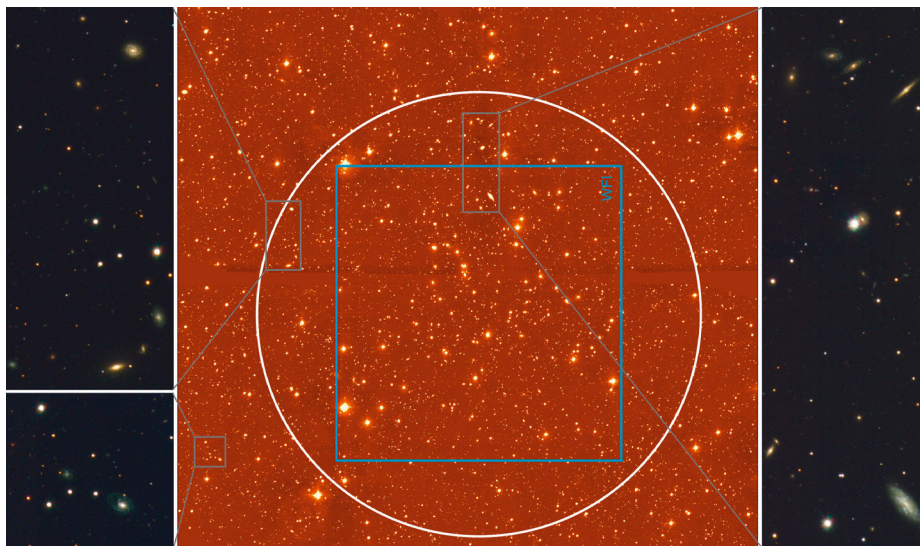


Figure 2. 1 by 1 degree V -band OmegaCAM image of cluster A2399. The FoV of WINGS imaging obtained with WFI is shown for comparison (grey square). The circle shows the radius (R_{200}) of the cluster. The colour images zooming into three selected areas were obtained by combining OmegaWINGS u -, B - and V -band images.

Data reduction

Image reduction and calibration are mainly based on the ESO/MVM (Multi-resolution Vision Model) reduction package (also known as ALAMBIC). This is a multi-instrument reduction tool originally developed for the ESO Imaging Survey (EIS). It has been extensively used also in the production of ESO Advanced Data Products (see for instance the 30 Doradus/WFI Data Release or the GOODS/ISAAC Final Data Release). A detailed description of the package and the documentation of the algorithm structure implemented in ESO/MVM are given in Vandame et al. (2004). There are configuration files for

many optical and near-infrared ESO instruments, but so far OmegaCAM is not officially supported. We therefore created a new configuration file for OmegaCAM, using the instrument description given in the VST user manual. We also developed a few modifications to the ALAMBIC pipeline in order to take into account OmegaCAM-specific issues, namely crosstalk correction, gain harmonisation and the control procedure that checks the quality of CCD #82 and masks it out should it not have worked properly during the observations (for details see Gullieuszik et al. [2015]).

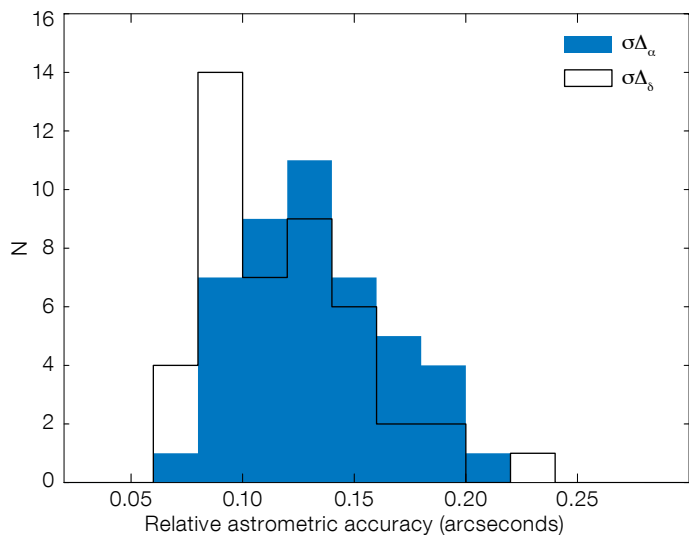
OmegaCAM detectors suffer electronic crosstalk. The strongest effect, of the order of a few percent, is between CCDs #95 and #96, located in a corner of the camera mosaic. The crosstalk has been estimated by cross-correlating the signal registered on the same pixel in each pair of CCDs. The crosstalk on CCD #95 and #96 is 0.3% and -0.8%, respectively.

Our analysis confirms that the effect on the other detectors is negligible. After correcting all images for crosstalk we performed the standard pre-reduction of all science frames, using ALAMBIC algorithms to subtract the bias and apply flat-field corrections.

The electronic converters of each detector are different, and each CCD may have a different efficiency. Therefore, each detector has its own effective gain and, as a consequence, its own photometric zero-point. The chip-to-chip gain variation quoted in the OmegaCAM User Manual is of the order of 10%, resulting in a chip-to-chip zero-point scatter of ~ 0.1 mag. We could not apply the standard procedures adopted by ALAMBIC to manage this problem, because of the central cross-shaped vignetting affecting OmegaCAM images taken with the segmented B and V Johnson filters. We therefore developed a variation of the original ALAMBIC procedure optimised for our specific OmegaCAM observations (see Gullieuszik et al. [2015] for details).

A well-known problem affecting wide-field cameras in particular is sky concentration, i.e., a stray-light component that is centrally concentrated. The net result is an erroneous apparent trend of the photometric zero point with the distance

Figure 3. Dispersion of the distributions of sky-coordinate differences between OmegaWINGS and WINGS positions of all stars in each of the 46 OmegaWINGS fields. Only stars brighter than $V = 20$ were used for the comparison.



from the centre of the camera field of view. We corrected for this effect by deriving an illumination map from observations of a well-populated stellar field, namely Landolt SA107. The illumination map was used to correct all science frames and to obtain photometrically flat, reduced science stacks.

Astrometric calibration was performed for all frames using the 2 Micron All Sky Survey (2MASS) catalogue as reference, or the Sloan Digital Sky Survey (SDSS) Data Release 8, when available. The absolute accuracy — measured on the final stacked mosaic — is of the order of 0.2 and 0.07 arcseconds for calibrations based on 2MASS and SDSS, respectively.

Photometric catalogues

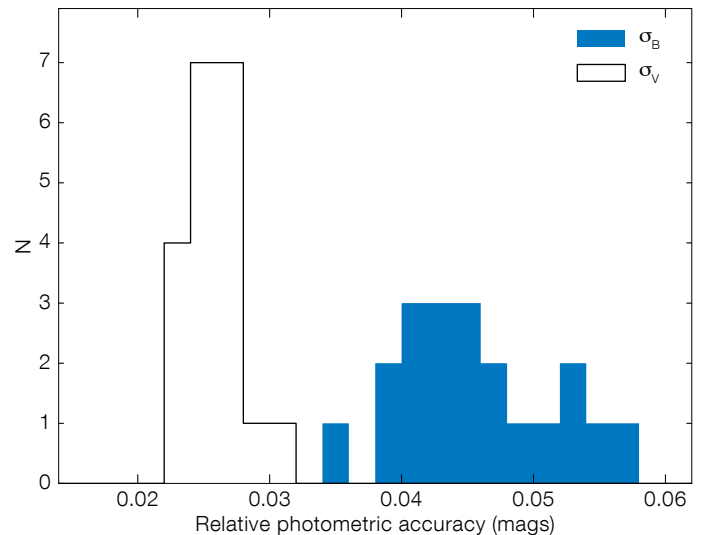
The source extraction and measurement of photometric and structural parameters was performed using SExtractor and by using WINGS stars as photometric local standards. The classification of OmegaWINGS sources was done following the method and criteria used for the original WINGS survey. As a starting point, we classified objects on the basis of the SExtractor star/galaxy classification parameter. We then used a set of diagnostic plots, using different combinations of SExtractor parameters (e.g., magnitude, full width at half maximum, isophotal area, central surface brightness) to check the result and correct any misclassification. During the visual inspection of the

diagnostic plots, we removed saturated stars from our catalogues. The complete OmegaWINGS photometric database is available at CDS.

The quality of OmegaWINGS results was tested against the WINGS ones. For each target cluster, we analysed the distribution of the differences of the coordinates and magnitudes between the two sets of catalogues. The mean values of all the distributions were found to be always negligible, proving that no relevant systematics affect OmegaWINGS photometry and astrometry. The dispersion of the distributions of sky-coordinate differences $\Delta\alpha$ and $\Delta\delta$ between OmegaWINGS and WINGS positions of all stars in each of the 46 OmegaWINGS clusters are shown in Figure 3; this provides the precision of the astrometric calibration which is shown to be accurate at a level always better than 0.25 arcseconds. The mean values of the distributions in Figure 3 are 0.1 arcseconds for both right ascension and declination, perfectly matching the precision required for the purposes of our scientific project. We note that the internal accuracy of WINGS astrometry is ~ 0.2 arcseconds (Fasano et al., 2006).

We detected no significant systematic differences between OmegaWINGS and WINGS photometry. This result proves

Figure 4. Relative photometric accuracy based on a comparison with SDSS Data Release 9. The histograms show the dispersion of the distributions of differences between OmegaWINGS and SDSS photometry.



the reliability of the gain harmonisation and illumination correction procedures. The relative accuracy of OmegaWINGS photometry across the OmegaCAM FoV was tested by comparing OmegaWINGS photometry with SDSS photometry (transformed onto the standard BV photometric system). For each of the 20 OmegaWINGS fields observed by SDSS, we calculated the dispersion of the differences between OmegaWINGS and (transformed) SDSS magnitudes for all stars with $B < 20$ mag and $V < 19$ mag. Results are shown in Figure 4. In the V -band the relative photometric accuracy is 0.03 mag for all clusters, while it ranges between 0.04 and 0.06 mag in the B -band.

The systematically higher dispersion in the B -band is due to non-linear colour terms in the transformations from SDSS ugr to BV photometric systems and/or a dependence of the transformations on star metallicity/colour. We also checked the spatial stability of OmegaWINGS calibration by analysing the magnitude difference between OmegaWINGS and (transformed) SDSS photometry as a function of the position on the mosaic. We found that the OmegaWINGS photometric zero point is constant within a few hundredths of a magnitude across the whole mosaic, confirming that there are no residual systematic effects, possibly due to the illumination correction and/or gain harmonisation issues.

The overall OmegaWINGS photometric completeness factor was estimated by comparing the magnitude distributions (MD) of all sources in the OmegaWINGS and WINGS catalogues. The photometric depth depends on the seeing conditions during observations, but OmegaWINGS photometry is in general 0.5–1.0 mag shallower than the WINGS one. However, when OmegaWINGS observations were carried out with seeing 1.0 arcseconds, OmegaWINGS is as deep as (and in some cases deeper than) WINGS. The overall photometric depth of OmegaWINGS was estimated by stacking together all 45 MDs. Figure 5 shows that OmegaWINGS MD peaks at $V \sim 22.5$ mag and WINGS at $V \sim 23.4$ mag.

The completeness of OmegaWINGS photometry can be estimated as the ratio of OmegaWINGS to WINGS MDs.

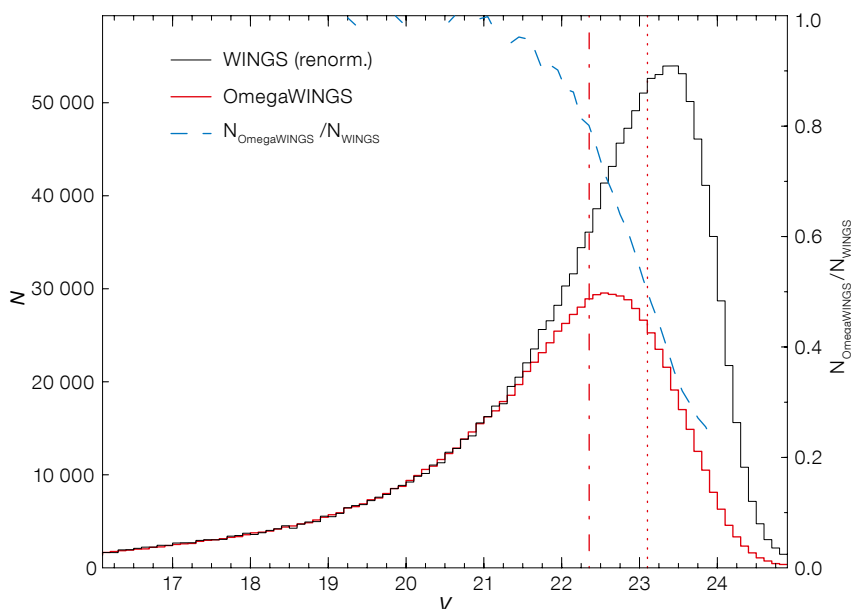


Figure 5. V -band magnitude distribution of all objects in the OmegaWINGS and WINGS database. The WINGS magnitude distribution was re-normalised to match the total number of OmegaWINGS sources with $16 < V < 21$ mag. The ratio of OmegaWINGS to WINGS distributions is shown as a dashed line; and the corresponding scale is shown on the right-hand axis. The vertical lines trace the magnitude corresponding to a ratio of 0.5 and 0.8 (50% and 80% completeness level), as dotted and dash-dotted lines respectively.

The 50% completeness level is reached at $V = 23.1$ mag, the 80% level at $V = 22.4$ mag (see Figure 5). This result is based on the assumption that WINGS photometry is complete at least up to $V \sim 23$ mag. We therefore performed a further test by fitting an exponential relation to the bright tail of the histogram in Figure 5. The completeness factor was obtained as the ratio of the observed MD to the best-fit exponential model. Following this approach, 50% and 80% completeness are found at $V = 23.3$ and 22.7 mag, respectively, confirming our results.

OmegaWINGS spectroscopy

A large spectroscopic follow-up campaign targeting OmegaWINGS clusters is ongoing with AAOmega on the AAT. We plan to obtain spectroscopy for $\sim 30\,000$ galaxies over the 1 square degree OmegaCAM fields. Our primary targets are galaxies in cluster regions

outside the cores where the contrast between cluster members and interloper density is lower and the measure of spectroscopic redshift is crucial to disentangle the cluster population.

From the OmegaWINGS data (OmegaCAM photometry and AAOmega spectroscopy), we will study all the main galaxy properties (morphological and structural parameters, colours and colour gradients within galaxies, star formation rates, history and stellar masses) in relation to their environment. The wide area covered by our survey will allow us to characterise the environment by both global conditions (such as cluster mass, X-ray luminosity and merger history) and local conditions (e.g., clustercentric distance, local density, substructures within clusters and structures surrounding clusters).

So far, we have secured high quality spectra for ~ 30 OmegaWINGS clusters, reaching very high spectroscopic completeness levels for galaxies brighter than $V = 20$ mag from the cluster cores to their periphery. Observations are still ongoing and we plan to complete the spectroscopic survey in a few semesters.

Ongoing scientific activity

The OmegaWINGS photometric catalogues (available at CDS) are presented in

Gullieuszik et al. (2015), together with a detailed description of the survey and the data reduction procedures summarised here. The OmegaWINGS team is currently working to extend all the analyses that were developed for WINGS data to OmegaWINGS (out to the virial radius and beyond). In particular, for each galaxy we will measure the local density, the morphological type (MORPHOT: automatic Galaxy Photometry; Fasano et al., 2015), the surface photometry parameters (GASPHOT: Galaxy Automatic Surface Photometry; D’Onofrio et al., 2014), redshift, star formation history and stellar mass (Fritz et al., 2014). A number of papers are in preparation to present and release these OmegaWINGS advanced data products. We will also release an updated version of the complete WINGS database through the virtual observatory interface, including OmegaCAM images (see Moretti et al. [2014] for a description of the WINGS database).

The wide area covered by OmegaWINGS observations allows coverage of the entire cluster extension and moreover strongly enhances the possibility of detecting and studying a statistically significant number of exotic objects. As an example, the OmegaWINGS survey has been used to carry out the first systematic search for galaxies undergoing gas stripping and, in particular, jellyfish galaxies (Poggianti et al., 2015). These are galaxies that exhibit tentacles of debris material suggestive of gas removal mechanisms, such as ram-pressure stripping (an example is shown in Figure 6). As such, they can be used to assess the relevance of gas removal processes from galaxies, to study how, where and why gas stripping occurs, and to investigate the consequences of this phenomenon on the galaxy star formation history and on the build-up of the intra-cluster/intra-group medium.

WINGS imaging was also used to cover clusters in the northern hemisphere, while the Padova–Millennium Galaxy and Group Catalogue (PM2GC; Calvi et al., 2011), based on the Millennium Galaxy Catalogue (Liske et al., 2003) was used to study jellyfish galaxies in low density environments. The jellyfish catalogue presented in Poggianti et al. (2015) consists of almost 400 candidates in ~ 70

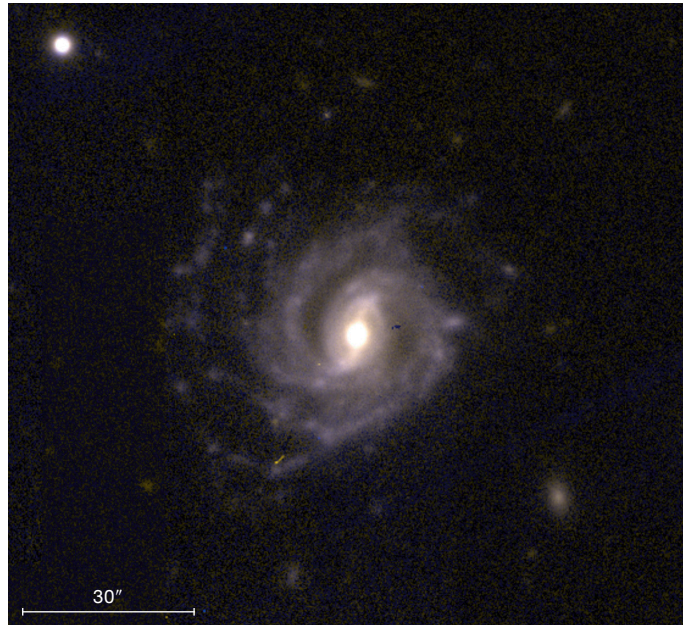


Figure 6. 2 by 2 arc-minute OmegaWINGS colour image of a jellyfish galaxy (Poggianti et al., 2015) in the cluster A2589.

galaxy clusters of the OmegaWINGS + WINGS sample, and about 100 candidates in groups and lower-mass structures in the PM2GC sample, all at redshift between 0.04 and 0.07. This is the largest sample of stripping candidates known to date.

While all jellyfish galaxies previously known from the literature are in clusters, we also found striking jellyfish candidates outside clusters, in groups and lower-mass haloes of the PM2GC sample, with masses between 10^{11} and $10^{14} M_{\odot}$. These results deserve further investigation in order to fully understand the role and the cause of gas stripping in groups, its impact on galaxy evolution in general and on the global quenching of star formation. Our sample comprises stripping candidates of all stellar masses, from $10^9 M_{\odot}$ to $10^{11.5} M_{\odot}$, indicating that whatever causes the jellyfish phenomenon can affect galaxies of any mass.

To reveal the physical process responsible for gas removal in these galaxies, integral field spectroscopy (IFS) observations are required. These observations would in fact provide a measurement of the stripping timescale and the star formation rate in the stripped gas, unambiguously identifying the physical process responsible for the gas outflow and enabling directly the study of the effects on

the evolution of the galaxy. Integral field spectroscopy with the Multi Unit Spectroscopic Explorer (MUSE) on the VLT was obtained for two of our OmegaCAM jellyfish galaxies. These data spectacularly reveal the emission lines (H β , [O III], [N II], H α and [S II]) associated with the ionised gas in the trails, out to several tens of kiloparsecs from the galaxy (Jaffé et al., in prep.). A larger IFS study on a statistically significant subsample of our jellyfish galaxies would unveil the rich physics and implications of the stripping phenomenon in galaxies as a function of galaxy environment and galaxy mass.

References

- Calvi, R., Poggianti, B. & Vulcani, B. 2011, MNRAS, 416, 727
D’Onofrio, M. et al. 2014, A&A, 572, A87
Ebeling, H. et al. 2000, MNRAS, 318, 333
Fasano, G. et al. 2006, A&A, 445, 805
Fasano, G. et al. 2015, MNRAS, 449, 3927
Fritz, J. et al. 2014, A&A, 566, A32
Gullieuszik, M. et al. 2015, A&A, accepted, arXiv:1503.02628
Liske, J. et al. 2003, MNRAS, 344, 307
Moretti, A. et al. 2014, A&A, 564, A138
Poggianti, B. M. et al. 2015, ApJS, submitted, arXiv:1504.07105
Vandame, B. 2004, PhD thesis, Université de Nice

Links

- ¹ WINGS website: <https://sites.google.com/site/wingsomegawings>

The SINFONI Nearby Elliptical Lens Locator Survey (SNELLS)

Russell J. Smith¹
John R. Lucey¹
Charlie Conroy²

¹ Centre for Extragalactic Astronomy,
Durham University, United Kingdom
² Harvard Smithsonian Centre for Astro-
physics, Cambridge, USA

The SINFONI Nearby Elliptical Lens Locator Survey (SNELLS) is a novel search for strong gravitational lenses among the local early-type galaxy population (redshift $z_{\text{lens}} < 0.055$). Observations of lensing by nearby galaxies can provide especially robust measurements of stellar mass in galaxies, with minimal corrections for dark matter contributions. In turn this leads to constraints on the initial mass function (IMF), i.e., the relative number of stars as a function of their mass at birth. To date, we have discovered two new multiple-image systems, and recovered the one previously known example. Analysing all three systems, we find the mean stellar mass-to-light ratio in these very massive early-type galaxies is consistent with a Milky Way IMF, in contrast to the “heavy” IMFs derived for ellipticals in some recent studies.

Nearby lenses as IMF probes

The stellar initial mass function controls a multitude of galaxy properties, including their evolving luminosities, supernova rates, element abundances, content of exotic stellar remnants, etc. The IMF is also the key output from theoretical star formation models. The question whether all stars are formed according to the same IMF as in the Milky Way thus has broad relevance to many fields of astrophysics.

The spectra of giant elliptical galaxies, which formed most of their stars in intense bursts at high redshift, show signatures of an excess of low-mass stars, indicating a “bottom heavy” IMF compared to the Milky Way (Conroy & van Dokkum, 2012). Measurements of large stellar mass-to-light ratios (M_{\star}/L), via lensing (e.g., Treu et al., 2010) and dynamical (e.g., Cappellari et al., 2013) analyses

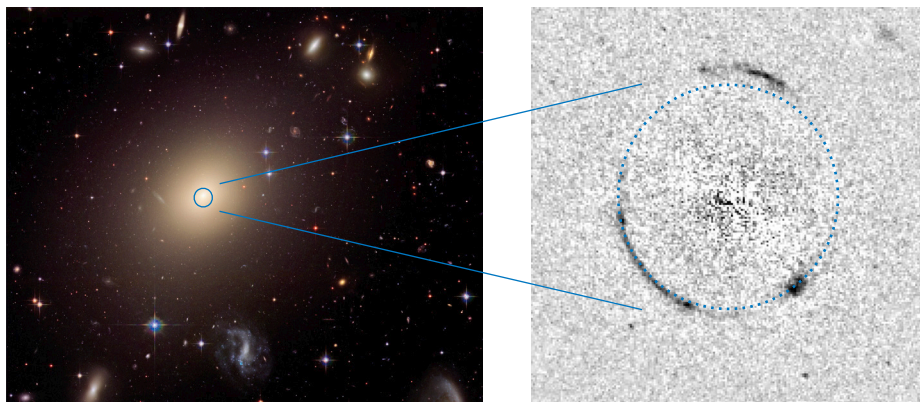


Figure 1. HST imaging of ESO325-G004, the only low-redshift strong-lensing elliptical galaxy known prior to the SNELLS programme. The left panel shows a colour composite (filters F475W, F625W, F814W) from the Hubble Heritage project.

The right panel shows the $z = 2.14$ gravitationally lensed arcs (F475W data after subtracting a smooth model for the foreground lens). The Einstein radius is shown by the blue circle.

seem to support this result on average, although careful comparison reveals substantial scatter at a galaxy-by-galaxy level, and differences in the trends with mass (Smith, 2014).

Galaxy-scale strong gravitational lensing can provide robust measurements of the total mass in galaxies, with errors of only a few percent in favourable cases. With no dependence on the dynamical or thermal state of tracer material, lensing is free from many of the degeneracies afflicting other mass probes. The most challenging step in deriving IMF constraints from such measurements is to estimate the fraction of the lensing mass comprised by stars, rather than dark matter. In “typical” lens systems, where the deflector galaxy is at $z = 0.2-0.5$, the dark and stellar components contribute comparable mass within the Einstein radius, R_{Ein} . As a result, IMF variations are hard to decouple from modifications to the inner dark matter halo profile, e.g., halo “contraction” in response to the stellar component.

The sensitivity of lensing-based IMF estimates to the dark matter component can be reduced by analysing lenses at lower redshift, where R_{Ein} is generally smaller, compared to the effective radius of the stellar distribution. Another advantage of low-redshift lenses is that detailed follow-up observations can be made to characterise other relevant properties, e.g., high signal-to-noise (S/N) spectra for

age and metallicity estimates, spatially resolved spectroscopy for detailed dynamical modelling, etc.

Until recently, however, there was only one confirmed strong-lensing giant elliptical at $z < 0.1$. ESO325-G004 was identified as a lens through high-resolution imaging with the Hubble Space Telescope (HST), which revealed a system of arcs forming a partial Einstein ring (Figure 1). The redshift of the arcs was measured with X-shooter, securing a measurement of the total mass within R_{Ein} (blue circle in Figure 1, left). After correction for the small dark-matter component, the estimated stellar mass-to-light ratio M_{\star}/L is found to be compatible with a Milky Way IMF (Smith & Lucey, 2013).

The results for ESO325-G004, and the apparent contrast with evidence for heavy IMFs in such galaxies, prompted us to begin a search for other strong lenses among the low-redshift ellipticals. Our aim is to construct a statistically useful sample of nearby lenses, with which to test for variations in the IMF in massive ellipticals as compared to the Milky Way.

An infrared integral field lens search

The characteristics of our search method can best be described through comparison to the Sloan Lensing ACS Survey (SLACS), introduced by Bolton et al. (2006). SLACS was a very successful

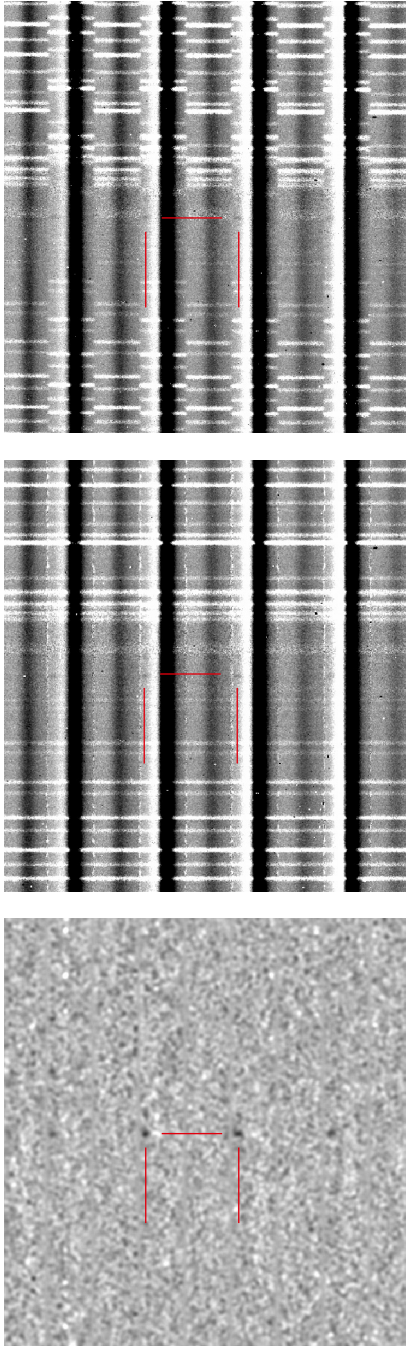


Figure 2. Detection of emission lines from the SNELLS data. The first panel shows a small section of the raw A - B difference image from the observation of SNL-1. Parts of nine image slices are visible. The lens galaxy produces the bright positive and negative vertical traces; horizontal lines are residual sky. The second panel shows the reduced difference image after wavelength calibration. The third panel shows the “detection” image, after removing residual sky and lens galaxy signals, normalising by the noise, filtering bad pixels, and smoothing. The $H\alpha$ emission line at $z = 0.926$, inconspicuous in the upper panels, is readily detected after this additional processing.

spectroscopic lens discovery programme, based on detecting anomalous background emission lines in Sloan Digital Sky Survey (SDSS) fibre spectra. Searching $\sim 10^5$ potential lenses, a total of 84 systems were identified as suitable for lensing analysis, after confirmation with HST imaging. The survey yield is thus one lens per ~ 1000 observed candidates.

An important limitation of the SLACS approach is its use of a single “global” spectrum derived from the SDSS fibre aperture: the faint lensed arc emission is observed against the whole integrated spectrum from the bright foreground galaxy, reducing contrast so that only systems with bright arcs can be detected. Since such lenses are rare, large volumes must be searched, with the result that SLACS samples rather distant galaxies, with $z_{\text{lens}} = 0.2\text{--}0.3$.

In SNELLS, we overcome this contrast problem by using integral field unit (IFU) data to concentrate the source flux spatially as well as spectrally. Since the lensed images are typically 1–3 arcseconds from the lens galaxy centre, the IFU allows us to detect arcs against a lower continuum brightness than in a single-fibre spectrum. Hence, we can detect more numerous (though less spectacular) faint sources. By using SINFONI (the VLT Spectrograph for Integral Field Observations in the Near Infrared) to observe in the near-infrared (NIR), we open up a larger search volume for $[O\ III]$ and $H\alpha$ emission lines behind each lens, as compared to the optical range, further increasing the number of detectable lens systems.

The SLACS search method has the inherent advantage of using pre-existing archival survey data, and hence incurring no new observational cost (although HST imaging follow-up is needed to model the lenses). In contrast our method requires new targeted observations, so we maximise discovery efficiency by pre-selecting the most promising lens candidates based on velocity dispersion, σ , as lensing cross-section scales as $\sim \sigma^4$.

Taken in combination, the heightened contrast (from the IFU), the greater search volume (from working in the NIR) and the increased efficiency (from targeting high- σ galaxies) leads to a much larger

survey “yield” than for the SLACS method. Calculating from the evolving $H\alpha$ luminosity function of Sobral et al. (2013), we predicted that our survey would be able to discover one lens per ~ 10 observed candidates, per hour of total exposure with SINFONI.

Implementation in ESO Period 93

For Period 93 we compiled a target sample using velocity dispersion data from the SDSS (Abazajian et al., 2009) and the 6dF Fundamental Plane Survey (Campbell et al., 2014). Candidate lenses were selected to have $z < 0.055$ and $\sigma > 300$ km s^{-1} . All targets were vetted to exclude objects with strong emission lines, unusual morphology, etc. We also rejected central cluster galaxies, which have much larger halo dark matter contributions; they are poor systems from which to estimate the stellar masses and are hence less suitable for use in constraining the IMF.

From a proposed sample of 36 galaxies, observations were acquired in J - and H -bands for 27 targets, including the previously known lens, ESO325-G004. We use the largest SINFONI image scale, delivering an 8 by 8 arcsecond field of view (cf., the expected Einstein radii of 2–3 arcseconds). A complete observation consists of two pointings, offset by 2.3 arcseconds, in J -band and two in H -band, with a single 600-second exposure in each pointing, per band.

After standard data reduction with the SINFONI pipeline, we perform additional processing to suppress the signal from the lens galaxy, as well as from the sky airglow lines. We identify emission lines through visual inspection of a two-dimensional signal-to-noise spectrum in “unwrapped cube” format (see Figure 2). For objects where emission peaks are detected, we construct narrowband images from the datacube, to locate the source, and extract spectra to determine the redshift.

Two new lenses, and an old one

In three of the candidates observed so far, we recover multiple emission-line sources with identical wavelengths

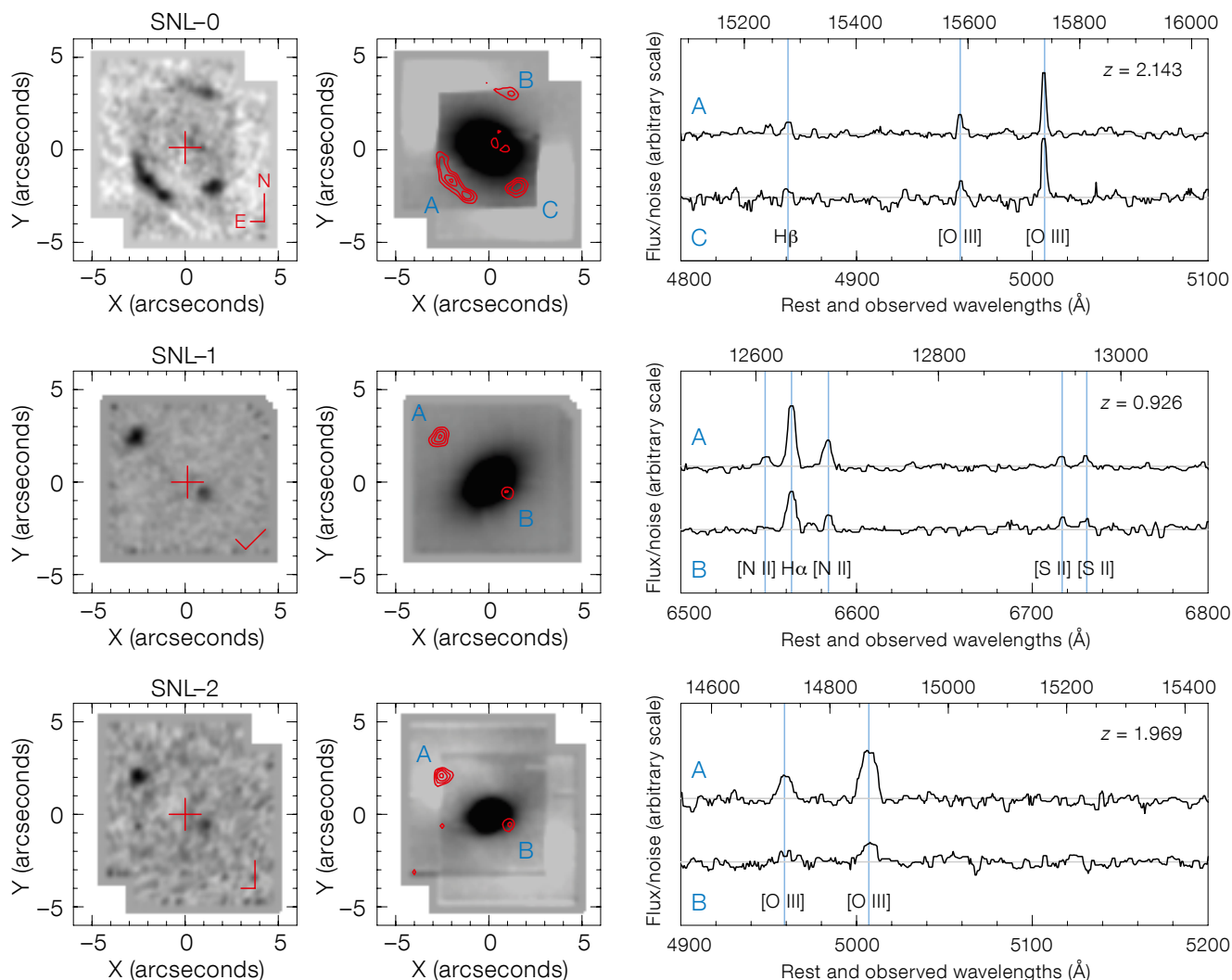


(Figure 3). The interpretation of these systems as strong gravitational lenses is compelling. The delivered survey yield is thus consistent, so far, with our predicted “one-in-ten” discovery rate. Details of the three systems (SNL-0 to SNL-2) follow.

SNL-0 (ESO325–G004)

This system is the previously known low-redshift lensing elliptical, to which we assign the name SNL-0 within SNELLS. Although this galaxy was well studied in our earlier work, it was retained as a SINFONI target to test our search methods on a lens with known properties.

The SNELLS data for SNL-0 are shown in the top row of Figure 3. The emission-line image recovers most of the structure of the arc system as seen in HST images (compare with Figure 1, right), though some fidelity is lost through combining

only two offset frames. The spectra show the strong [O III] 4959, 5007 Å doublet and weak H β line, as seen in X-shooter data (Smith & Lucey, 2013). No other lines were detected.

SNL-1 (ESO286–G022)

SNL-1 is an isolated, very compact galaxy, with an effective radius of only 2 kpc, but a total luminosity of $\sim 1 \times 10^{11} L_{\odot}$ in the J -band. SuperCOSMOS and 2 Micron All Sky Survey (2MASS) images show an elongated but otherwise featureless morphology. The 6dF spectrum suggests an old passive stellar population, with weak H γ and H β absorption, and no emission detectable at H α or elsewhere.

As the first new discovery from SNELLS, the original data were supplemented with deeper Director’s Discretionary Time

(DDT) observations to confirm this galaxy definitively as a lens. SINFONI reveals a doubly imaged emission-line source in the J -band; additional lines confirm the source is H α at a redshift of $z = 0.926$ (Figure 3, second row). The emission line sources are spatially unresolved in the SINFONI data. With $z_{\text{lens}} = 0.031$, SNL-1 is now the closest confirmed galaxy-scale strong lens. From Smith et al. (2015).

(DDT) observations to confirm this galaxy definitively as a lens. SINFONI reveals a doubly imaged emission-line source in the J -band; additional lines confirm the source is H α at a redshift of $z = 0.926$ (Figure 3, second row). The emission line sources are spatially unresolved in the SINFONI data. With $z_{\text{lens}} = 0.031$, SNL-1 is now the closest confirmed galaxy-scale strong lens.

SNL-2 (2MASX J01414232–0735281)

This object, with $z_{\text{lens}} = 0.052$, is part of a galaxy pair, with a fainter companion 7 arcseconds to the north (beyond the SINFONI field of view). SDSS imaging shows a faint outer envelope around both galaxies. SNL-2 itself has very regular morphology; its effective radius (6 kpc) and total luminosity ($\sim 3 \times 10^{11} L_{\odot}$ in J -band) are comparable to those of SNL-0. The 6dF spectrum is consistent with a pure passive stellar continuum.

The SNELLS data reveal emission in two noticeably broad emission lines consistent with the [O III] 4959, 5007 Å doublet, at a redshift of $z = 1.969$ (Figure 3, bottom row). The lines form two spatially unresolved images, quite similar to the case of SNL-1. No counterpart to the emission-line source is visible in the SDSS imaging.

IMF constraints

We apply simple lensing models for each galaxy to determine the Einstein radius, R_{Ein} , and the corresponding total projected mass, M_{Ein} . The total lensing masses have estimated precision of 5% for SNL-0 and SNL-1, and 10% for SNL-2, the latter being larger due to uncertainty in the shear from the companion galaxy.

To derive an estimate for the stellar mass within R_{Ein} , we estimate the dark matter contribution based on the projected halo mass profiles of similarly massive galaxies in the EAGLE cosmological hydrodynamical simulations (Schaller et al., 2015). Through this method, the dark matter fractions within R_{Ein} are estimated to be 16–26%. With the stellar mass-to-light ratio in hand, we compare against the predictions from stellar population synthesis models to determine the deviation of the IMF from a fiducial Kroupa (2001) case. We quantify the IMF constraint through the mass excess factor α , which is the ratio of measured M_{\star}/L to the value expected under the fiducial IMF. This step requires knowledge of the stellar population age. Our “default” assumption is that these very massive ellipticals formed all their stars at early epochs, with an age 10 ± 1 Gyr (formation redshift $1 < z < 4$, at two standard deviations).

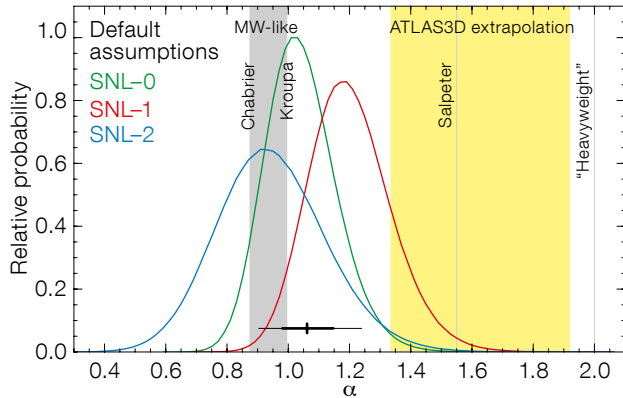


Figure 4. Constraints derived from the three SNELLS lenses for our “default” assumptions (see text). α is the mass excess factor, relative to a Milky Way IMF. The heavy/light bar below shows the $1\sigma/2\sigma$ intervals for the mean of the three SNELLS galaxies. All three galaxies have a mass-to-light ratio consistent with a Kroupa IMF. For comparison, the yellow shading indicates $\pm 1\sigma$ in α expected at the mean velocity dispersion of our sample, 345 km s^{-1} , based on the trend reported by Cappellari et al. (2013). From Smith et al. (2015).

Under our standard assumptions, we derive IMF mass excess factors of $\alpha = 1.04 \pm 0.11$, 1.20 ± 0.13 and 0.94 ± 0.17 , for SNL-0, SNL-1 and SNL-2, respectively (see Figure 4). After a small correction for selection bias caused by the SINFONI field of view, the estimated mean is $\langle \alpha \rangle = 1.06 \pm 0.08$ (the quoted error is statistical; there is also a ± 0.10 systematic component which applies to all results here). Hence, individually, and on average, the lensing constraints for these three very massive ellipticals are consistent with a Milky Way IMF, old stellar populations and EAGLE dark matter profiles.

We have explored various modifications to our methodology and assumptions, finding that the preference for a standard IMF is quite robust. For example, if the stellar age of each galaxy is fit directly from the optical spectrum, instead of being assumed “old”, we recover $\langle \alpha \rangle = 1.19 \pm 0.15$ after bias correction. This average is still consistent with the Kroupa (2001) IMF. Alternatively, if we assign all of the lensing mass to the stars, i.e., assume negligible dark matter, we find a mass excess of $\langle \alpha \rangle = 1.31 \pm 0.09$, still smaller the value of 1.55 expected for a Salpeter power law IMF.

These results are surprising, given the accumulated evidence for “heavy” IMFs in massive ellipticals from other studies. For example, to reproduce the gravity-sensitive spectral features in such galaxies, Conroy & van Dokkum (2012) require an IMF with an excess of cool dwarf stars, implying a large M_{\star}/L , and $\alpha \sim 2$ in the most massive galaxies. From the SLACS lenses, Treu et al. (2010) derived $\alpha \sim 2$ at $\sigma > 300 \text{ km s}^{-1}$; from dynamical

modelling of galaxies in the ATLAS3D survey, Cappellari et al. (2013) recover $\alpha \sim 1.5$ on average at high σ .

The causes of these apparent discrepancies are not yet understood; inter-comparison between the various methods applied to the same set of galaxies will be crucial to resolving this puzzle. The SNELLS lenses provide a unique benchmark sample, for which the various methods (spectroscopic, dynamical and lensing) can all be applied, in bright nearby galaxies where excellent data quality can be obtained.

Ongoing work and prospects

The SNELLS lens search programme is continuing in Period 95, with an enlarged sample of candidates at $z_{\text{lens}} < 0.06$. Our aim is to double the number of low-redshift lenses, enabling us to: (a) provide tighter limits on the average α in very massive ellipticals; (b) determine the galaxy-to-galaxy scatter in α among such galaxies; and (c) test for correlations of α with other parameters (metallicity, compactness, etc.).

In parallel with the search programme, follow-up observations are underway to obtain uniform high-quality supporting data for the three lenses SNL-0, SNL-1 and SNL-2. With FORS2 we will acquire deeper and higher-resolution optical imaging than currently available for the three systems. Meanwhile, X-shooter will provide high-S/N spectroscopy over the full optical and NIR range, which will improve the direct constraints on stellar

ages (obviating the need to assume old populations). The X-shooter observations will also yield measurements for the IMF-sensitive spectral features (e.g., Na I, FeH, etc.) in the far-red and NIR, for direct comparison against the lensing results for the same galaxies.

SINFONI is currently the only near-infrared integral field unit, on any large telescope, with sufficient contiguous field of view to perform this kind of survey efficiently. In the long term, we anticipate that with HARMONI on the European Extremely

Large Telescope, it should be possible to detect faint lensed line-emitters behind any chosen massive elliptical, opening up the prospect of measuring strong-lensing masses “to order”, rather than as a matter of luck.

Further details

A full description of the Period 93 lens search and our IMF results can be found in Smith, Lucey & Conroy (2015).

Acknowledgements

RJS was supported by the STFC Durham Astronomy Consolidated Grant 2014–2017 (ST/L00075X/1).

References

- Abazajian, K. N. et al. 2009, *ApJS*, 2009, 182
 Bolton, A. S. et al. 2006, *ApJ*, 638, 703
 Campbell, L. et al. 2014, *MNRAS*, 433, 1231
 Cappellari, M. et al. 2013, *MNRAS*, 432, 1862
 Conroy, C. & van Dokkum, P. 2012, *ApJ*, 760, 71
 Kroupa, P. 2001, *MNRAS*, 322, 231
 Schaller, M. et al. 2015, *MNRAS*, 451, 5765
 Sobral, D. et al. 2013, *MNRAS*, 428, 1128
 Smith, R. J. 2014, *MNRAS*, 443, L69
 Smith, R. J. & Lucey, J. R. 2013, *MNRAS*, 434, 1964
 Smith, R. J., Lucey, J. R. & Conroy, C. 2015, *MNRAS*, 449, 3441
 Treu, T. et al. 2010, *ApJ*, 709, 1195

NASA, ESA, ESO and D. Coe (STScI)/J. Meisen (Heidelberg/Bologna)



Composite image (FORS1 *V*, *R* and *I* filters and Hubble Space Telescope *B*, *V*, *I*) of the galaxy cluster Abell 2744 (redshift 0.31), one of the Hubble Frontier Fields clusters. Abell 2744 is one of the most actively merging galaxy clusters and shows evidence of several merger events with prominent X-ray and dark matter substructures. Many background high redshift galaxies amplified by the gravitational lensing of the cluster have been identified.

The ESO UVES Advanced Data Products Quasar Sample: Neutral Gas Mass and Metal Abundances in the Universe

Tayyaba Zafar¹
 Céline Péroux²
 Giovanni Vladilo³
 Miriam Centurión³
 Paolo Molaro³
 Valentina D’Odorico³
 Kumail Abbas⁴
 Attila Popping⁵
 Bruno Milliard²
 Jean-Michel Deharveng²
 Stephan Frank^{2,6}

¹ ESO

² Aix Marseille Université, CNRS, Laboratoire d’Astrophysique de Marseille (LAM), France

³ INAF — Osservatorio Astronomico di Trieste, Italy

⁴ Center of Excellence in Solid State Physics, University of the Punjab, Lahore, Pakistan

⁵ International Centre for Radio Astronomy Research (ICRAR), The University of Western Australia, Crawley, Australia

⁶ Department of Astronomy, Ohio State University, Columbus, USA

Damped Ly α absorbers (DLAs), seen in the spectra of background quasars, are unique probes to select HI-rich galaxies. We selected a dataset of 250 quasars observed with the Ultraviolet Visual Echelle Spectrograph (UVES) and available through the ESO UVES Advanced Data Products (EUADP) archive, to study the gas and metal properties of 150 damped absorbers. These high-redshift absorbers contain information on the physical state and chemical composition of the interstellar medium and the neutral gas mass, a possible indicator of gas consumption as star formation proceeds. We find no evolution of the neutral gas mass density, with sub-DLAs contributing 8–20 % (increasing with redshift). The EUADP dataset provides insights into the nucleosynthetic origin of nitrogen, confirming the bimodal behaviour of $[N/\alpha]$, and also confirms the deficiency of argon in DLAs.

Motivation

The study of quasar absorbers has contributed new insights into the field of galactic evolution research. The damped

Ly α absorbers ($N_{\text{HI}} \geq 2 \times 10^{20} \text{ cm}^{-2}$) and sub-DLAs ($10^{19} \leq N_{\text{HI}} \leq 2 \times 10^{20} \text{ cm}^{-2}$; Péroux et al., 2005) contain a large fraction of neutral hydrogen in the Universe. DLAs are believed to be major contributors of the neutral gas in the Universe, so their study is an important tool for understanding the structure of young galactic systems. DLAs are frequently used as tracers of cosmic chemical evolution, despite the fact that their nature and morphology is still not clear. The metallicity distribution over cosmic time provides clues on the degree of chemical enrichment, the onset of initial star formation and the nature of galaxies.

We have collected UVES high-resolution quasar spectra taken between February 2000 and March 2007 and available in the EUADP archive, giving a sample of 250 quasar spectra (ranging from $0.2 < z < 6.3$). The total VLT–UVES exposure time of this dataset is 1560 hours. The individual quasar spectra have been carefully merged and normalised. To derive a complete census of DLAs/sub-DLAs both an automated and visual inspection have been undertaken, leading to a sample of 93 DLAs and 57 sub-DLAs. An extensive search in the literature indicated that 19 DLAs/sub-DLAs have had their HI column densities measured for the first time; four DLAs and six sub-DLAs are new identifications (see Zafar et al., 2013a).

The motivation behind the project is to obtain a complete picture of the redshift evolution of both the cosmological neutral gas mass density and the metal content of the Universe using both DLAs and sub-DLAs. Moreover, this dataset will help to perform studies of metal abundances, molecules, and advance understanding of the elemental nucleosynthetic origin. In addition, these studies will demonstrate the properties and environments of quasar absorbers. In this article, we summarise the early results from the EUADP dataset.

Neutral gas mass density

Baryons comprise a small fraction of the critical matter–energy density of the Universe with $\Omega_b h^2 = 0.02205 \pm 0.00028$. In recent years, new observations have considerably changed the global picture

of the observable baryons in the Universe (e.g. Shull et al., 2012; Noterdaeme et al., 2012). In their neutral and molecular phases, baryons are the reservoirs of gas from which stars form. The HI clouds form molecules and molecular clouds further cool, fragment, and initiate star formation in galaxies. The neutral gas mass density (Ω_g) evolution over cosmological scales is a possible indicator of gas consumption as star formation proceeds. Ω_g observed in high-redshift quasar absorbers is expressed as a fraction of today’s critical density. The contribution of sub-DLAs to Ω_g was however poorly constrained until now (see Péroux et al., 2005). Simulations indicate that the gas in sub-DLAs is located in extended halos, whereas the gas in DLAs is located in dense and compact regions (van de Voort et al., 2012). DLAs/sub-DLAs provide the reservoir of neutral gas and serve as a barometer of recent star formation activity.

We have built a carefully selected subset of the EUADP dataset to study the statistical properties of DLAs and sub-DLAs, their column density distribution and the contribution of sub-DLAs to the gas mass density. We combined our DLA and sub-DLA statistical samples with the Péroux et al. (2003) and Péroux et al. (2005) samples respectively, for improved statistics. The details on building the statistical sample are provided in Zafar et al. (2013b). On account of the high spectral resolution of EUADP, the hydrogen column density distribution, $f_{\text{HI}}(N, z)$, down to $\log N_{\text{HI}} = 19.0$ is determined (Figure 1). The column density distribution, $f_{\text{HI}}(N, z)$, describes the evolution of quasar absorbers as a function of atomic column density and redshift.

The flattening of $f_{\text{HI}}(N, z)$ in the sub-DLA regime is present in the observations. We divided the $f_{\text{HI}}(N, z)$ distribution into two redshift bins of $1.5 < z < 3$ and $3 < z < 5$ (see Zafar et al., 2013b). A redshift evolution of $f_{\text{HI}}(N, z)$ is seen, indicating the presence of more sub-DLAs at high redshift compared to low redshift. Such an evolution suggests that sub-DLAs may merge and/or be more self-shielded with cosmic time. The behaviour of $f_{\text{HI}}(N, z)$ at six redshift bins (step increase of $z = 0.5$) is further used to determine the total HI gas mass density, Ω_g , between $1.5 < z < 5.0$. The results indicate

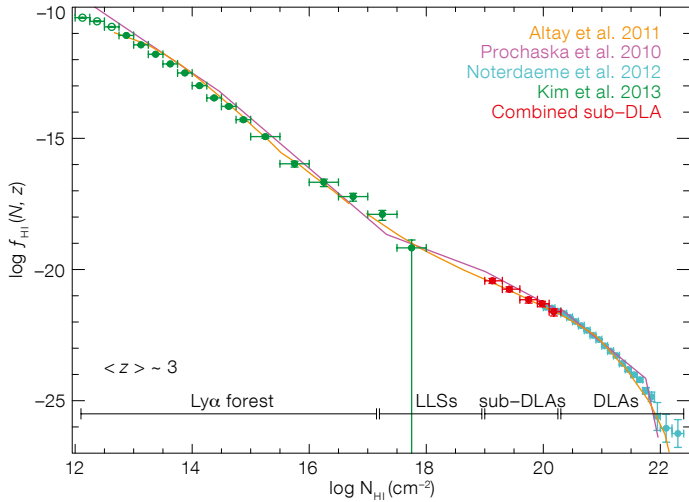


Figure 1. The column density distribution at $z \sim 3$ is plotted against $\log N_{\text{HI}}$ (from Zafar et al., 2013b). The red data points indicate $f_{\text{HI}}(N, z)$ for sub-DLAs. The green points represent $f_{\text{HI}}(N, z)$ for Ly α forest (Kim et al., 2013), the cyan points results from Noterdaeme et al. (2012) and the solid magenta line the estimation of $f_{\text{HI}}(N, z)$ at $z \sim 3.7$ using a series of six power laws by Prochaska et al. (2010). The solid orange line is the model prediction at $z \sim 3$ (Altay et al., 2011).

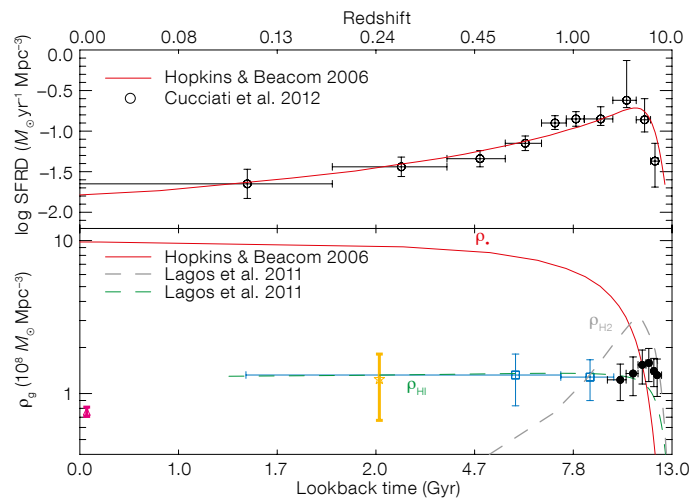


Figure 2. Upper panel: Total star formation rate (SFR) density as a function of lookback time (from Cucciati et al., 2012) is shown in black open circles. The red curve corresponds to the parametric form of the SFR density (Hopkins & Beacom, 2006). Lower panel: The black bins correspond to ρ_g measured from DLAs + sub-DLAs (Zafar et al., 2013b). See text for more details.

that sub-DLAs are important at all redshifts and their contribution to Ω_g increases from 8–20%, with an increasing fraction at higher redshift.

In the lower panel of Figure 2, the trend of the physical space density, ρ_g , measured from DLAs/sub-DLAs, with lookback time is plotted. The magenta triangle represents the result for local galaxies from Martin et al. (2010). The orchid star illustrates ρ_g measured from the star-forming galaxies (Lah et al., 2007). The blue squares represent measurements from Mg II selected DLAs (Rao et al., 2006). The dashed green and grey lines represent the prediction of ρ_g and ρ_{H_2} (Lagos et al., 2011), respectively. The solid red line illustrates the evolution of stellar mass density build-up inferred from the star formation history by Hopkins & Beacom (2006).

Figure 2 shows no evolution of Ω_g (or ρ_g) from low- to high-redshift with $\Omega_g \sim 1 \times 10^{-3}$ or $\rho_g \sim 1.4 \times 10^8 M_\odot \text{Mpc}^{-3}$. In contrast, star formation in galaxies steadily increases towards $z \sim 2.1$ by almost an order of magnitude (e.g., Cucciati et al., 2012). Given the star formation rate (SFR) density as function of redshift (Figure 2, upper panel), it is expected that HI plus H₂ gas at high redshift would be exhausted on timescales of few Gyr. However, the lack of evolution of Ω_g indicates that star formation alone cannot explain this non-evolution (Figure 2). Introduction of the continuous replenishment of gas through the accretion of matter from filaments and/or recombination of ionised gas in the walls of super-shells may help to sustain constant Ω_g over cosmic time (see Zafar et al., 2013b; Hopkins et al., 2008).

Evidence of bimodality in the nitrogen abundance distribution

The EUADP damped absorber dataset has been further used to understand the nucleosynthetic histories of nitrogen. N abundance determination in sites of low and high metallicities plays an important role in understanding its nucleosynthetic origin. The main pathway for the production of N in stars happens in the stellar H-burning layer, with the result that N is synthesised from C and O. Nitrogen has two production pathways, labelled either primary or secondary, depending on whether the seed C and O are produced by the star itself (primary) or were already present in the interstellar medium (ISM) out of which the star first condensed (secondary). Secondary production is the dominant process in the H-burning layers of intermediate-mass stars. Secondary production dominates at high metallicities ($[\text{O}/\text{H}] > -1$) and shows a correlation between (N/O) and (O/H) . At low metallicities, N goes in lock-step with O, so that (N/O) remains approximately constant.

Primary N production in intermediate-mass stars occurs from the synthesis of C and O freshly produced by the star in the He-burning shell during the asymptotic giant branch (AGB) phase (Henry et al., 2000). In the case of massive stars, the N production is very uncertain. At very low metallicities, only fast-rotating massive stars ($9 \leq M/M_\odot \leq 20$) can provide primary N (Chiappini et al., 2006). The discovery of metal-poor halo stars with high (N/O) ratios seems to confirm the primary N production in massive stars (Spite et al., 2005).

Measurements of N abundance have been performed in different astrophysical sites. In partly ionised, HII regions of spiral and dwarf irregular galaxies (van Zee et al., 1998), metal-poor emission line galaxies (Nava et al., 2006), and HII regions in blue compact dwarf (BCD) galaxies (Izotov & Thuan, 2004), (N/O) ratios show a primary plateau at low O abundances and a secondary behaviour for $[\text{O}/\text{H}] > -1$.

Studies of nitrogen in DLAs/sub-DLAs (spanning the broad metallicity range $-3.0 \leq Z/Z_\odot \leq -0.5$) provide important

clues of the earlier stages of galactic chemical evolution. We have estimated nine new neutral N (NI) measurements and nine limits in DLAs/sub-DLAs from the EUADP sample (see Zafar et al., 2014a). We combine these data with a careful reappraisal of literature high-resolution measurements published to date, making a sample of 108 systems. This is the largest N abundance sample studied so far.

We also derived $[N/\alpha]$ (where α is an α -chain element, either O, S or Si) abundance ratios for our sample. The extended sample confirms the bimodal behaviour of $[N/\alpha]$ suggested in previous studies. Three quarters of the systems show $\langle [N/\alpha] \rangle = -0.85 (\pm 0.20 \text{ dex})$ and one quarter are clustered at $\langle [N/\alpha] \rangle = -1.41 (\pm 0.14 \text{ dex})$. In Figure 3, the magenta diamonds and green pluses indicate measurements in the HII regions of spiral (van Zee et al., 1998) and BCD galaxies (Izotov & Thuan, 2004) respectively (with average error bars indicated in the top-left corner). The high $[N/\alpha]$ plateau is consistent with the HII regions of BCD and dwarf irregular galaxies, although extended to lower metallicities, and could be interpreted as the result of a primary N production by intermediate-mass stars (see Figure 3). The low $[N/\alpha]$ values are the lowest ever observed in any astrophysical site. These low abundances may indicate a primary N production from fast-rotating, massive stars in relatively young or unevolved systems.

Deficiency of argon in DLA systems

The EUADP dataset has been further used to determine the ionisation state of the gas at different redshifts using the “noble gas” argon. This element, with first ionisation potential 15.76 eV, is expected to be mostly neutral in interstellar HI regions, which are opaque to photons with energies just above the HI ionisation threshold (13.6 eV). The ionisation fraction of Ar is very sensitive to high energy ionising photons that are able to leak through the neutral gas. When the radiation field is hard, Ar is predicted to be deficient relative to other low ionisation species typical of HI regions. On the other hand, Solar-like abundances are expected when the ionising spectrum is

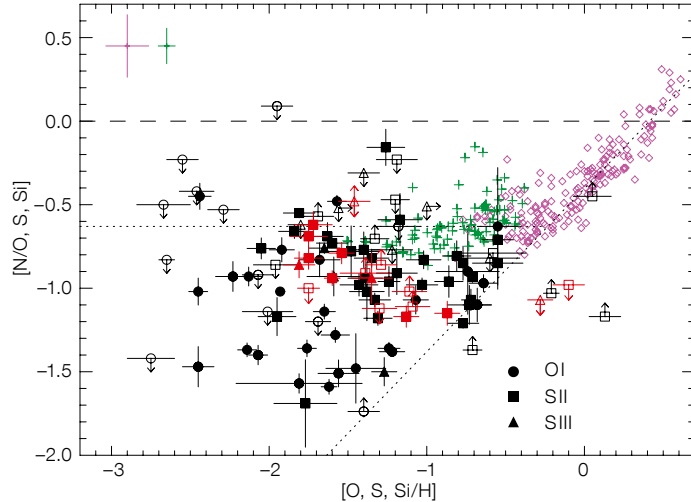


Figure 3. The $[N/\alpha]$ ratio determinations against metallicity. The circles, squares, and triangles indicate the O, S and Si abundances in DLAs/sub-DLAs, respectively (filled symbols: measurements; open symbols: limits). The red data points are the new estimates from Zafar et al. (2014a). Dotted lines are empirical representations of the secondary and primary N production. The dashed line indicates the Solar level.

soft. In the Galaxy, neutral argon is found to be deficient in low-density interstellar regions (Jenkins, 2013). However, owing to the saturation of neutral argon (Ar I) lines, Galactic studies can only probe regions with relatively low HI column density, typically associated with warm interstellar gas. On account of the low metallicities of the DLAs, the rare Ar I lines offer a way to probe the ionisation state of the neutral gas in high-redshift galaxies.

In Zafar et al. (2014b), we used the EUADP database to search for Ar I lines in DLAs/sub-DLAs. We made three new measurements and obtained five upper limits of Ar I. We combine these data with the literature high-resolution measurements, together comprising a total of 37 systems, i.e., the largest high-redshift Ar sample collected so far. We confirm that Ar is generally deficient in DLAs, with a mean value $[Ar/\alpha] = -0.4 \pm 0.06 \text{ dex}$ (with $\alpha = S \text{ or Si}$). The $[Ar/\alpha]$ ratios show a weak, positive trend with increasing HI column density and increasing absorption redshift, and a weak, negative trend with metallicity, $[S/H]$. Detailed analysis of the measured abundance ratios indicates that the Ar deficiencies are due to ionisation processes, rather than dust depletion or nucleosynthesis. Altogether, the observational evidence is consistent with a scenario of Ar ionisation dominated by the harsh radiation of quasars, modulated by local HI self-shielding inside the DLA host galaxies.

In principle, by measuring the ionisation state of the gas at different redshifts, we

can track the evolution of the co-moving density of cosmic sources and variations of the transparency of the intergalactic medium resulting from the processes of cosmic reionisation. Our measurements and limits of Ar abundance suggest that the cosmic reionisation of HeII takes place at redshift higher than $z \sim 3$ (see Figure 4), but more measurements at $z > 3.5$ are required to set firmer constraints on the redshift evolution of the HeII reionisation.

Conclusions and prospects

Quasar absorbers are a useful tool to study the gas and metal enrichment history of the Universe. We have made use of the Advanced Data Products archive recently made available to the community by ESO to study the largest sample of quasar echelle spectra available to date. The EUADP sample of DLAs and sub-DLAs allows estimation of the neutral gas mass over cosmological scales. No evolution of the neutral gas mass density is indicated, which we interpret as the accretion of gas on cosmological scales. The EUADP dataset confirms the bimodal behaviour of $[N/\alpha]$, inferring primary N production by intermediate-mass stars. The EUADP study further confirms the deficiency of Ar in damped absorbers, interpreted as an ionisation effect, which indicates that the cosmic reionisation of HeII is completed above $z \sim 3$.

Further works, including the metallicity of sub-DLAs as possible tracers of the

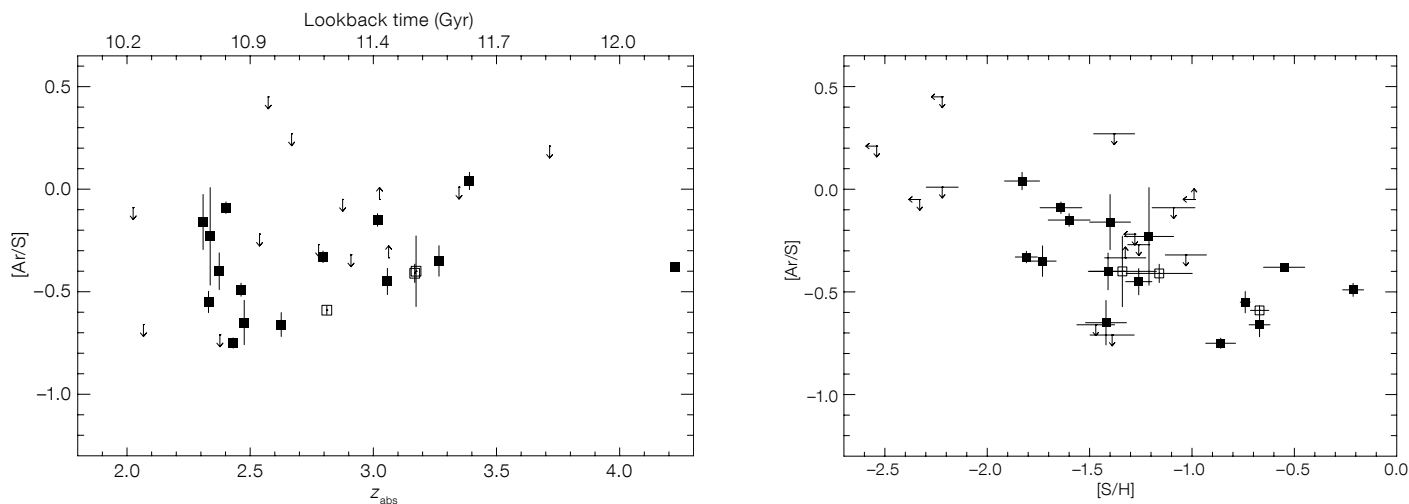


Figure 4. Left panel: The [Ar/S] ratio in DLAs plotted against redshift (bottom axis) and lookback time (top axis), for $H_0 = 70 \text{ km s}^{-1} \text{ Mpc}^{-1}$, $\Omega_m = 0.3$, and $\Omega_\Lambda = 0.7$. Right panel: The [Ar/S] versus S-based metallicities in DLA systems. A small amount of chemical evolution can be seen in [Ar/S]. In both panels, solid squares and arrows correspond to measurements and limits, respectively. The open squares illustrate proximate DLAs with $z_{em} \approx z_{abs}$ (see Zafar et al. [2011] for more details).

circum-galactic medium of galaxies (Quiret et al., in prep), are underway. Finally, since we started this study, the number of quasar spectra available in the UVES Advanced Data Products archives has more than doubled. Altogether, these

results illustrate the high scientific return of processed data archives.

References

Altay, G. et al. 2011, ApJ, 737, L37
 Chiappini, C. et al. 2006, A&A, 449, L27
 Cucciati, O. et al. 2012, A&A, 539, A31
 Henry, R. B. C., Edmunds, M. G. & Köppen, J. 2000, ApJ, 541, 660
 Hopkins, A. M. & Beacom, J. F. 2006, ApJ, 651, 142
 Hopkins, A. M., McClure-Griffiths, N. M. & Gaensler, B. M. 2008, ApJ, 682, L13
 Izotov, Y. I. & Thuan, T. X. 2004, ApJ, 602, 200
 Jenkins, E. B. 2013, ApJ, 764, 25
 Kim, T.-S. et al. 2013, A&A, 552, A77
 Lagos, C. D. P. et al. 2011, MNRAS, 418, 1649
 Lah, P. et al. 2007, MNRAS, 376, 1357

Martin, A. M. et al. 2010, ApJ, 723, 1359
 Nava, A. et al. 2006, ApJ, 645, 1076
 Péroux, C. et al. 2003, MNRAS, 345, 480
 Péroux, C. et al. 2005, MNRAS, 363, 479
 Prochaska, J. X., O’Meara, J. M. & Worseck, G. 2010, ApJ, 718, 392
 Rao, S. M., Turnshek, D. A. & Nestor, D. B. 2006, ApJ, 636, 610
 Spite, M. et al. 2005, A&A, 430, 655
 van de Voort, F. et al. 2012, MNRAS, 421, 2809
 van Zee, L. et al. 1998, AJ, 116, 2805
 Zafar, T. et al. 2011, A&A, 532, A51
 Zafar, T., Popping, A. & Péroux, C. 2013a, A&A, 556, A140
 Zafar, T. et al. 2013b, A&A, 556, A141
 Zafar, T. et al. 2014a, MNRAS, 444, 744
 Zafar, T. et al. 2014b, MNRAS, 445, 2093Z



B, V, R composite image of the barred spiral (SB) galaxy NGC 6300 taken with EFOSC2 on the New Technology Telescope (NTT). The active galactic nucleus of NGC 6300 is of Seyfert 2 type and displays rapidly variable hard X-ray emission. See Picture of the Week for 2 March 2015 for more information.

(Next page) Recent aerial view of the progress on levelling of the summit of Cerro Armazones in preparation for construction of the dome of the European Extremely Large Telescope.



ESO/G. Hudepohl (atacamaphoto.com)

Baryons at Low Densities: The Stellar Halos around Galaxies

held at ESO Headquarters, Garching, Germany, 23–27 February 2015

Marina Rejkuba¹
Magda Arnaboldi¹
Elena Valenti¹

¹ ESO

The workshop (Stellar Halos 2015) focused on theoretical and observational studies of the faint surface brightness envelopes surrounding luminous galaxies. This field of research has gained much attention in recent years owing to the availability of wide-field cameras, deep and large-area surveys, as well as advances in modelling galaxy formation and evolution. The comparison of the observational properties of stellar halos with the predictions from simulations provides important constraints on the formation of luminous galaxies and their assembly history. An overview of the topics covered at the workshop is presented.

Stellar halos are ubiquitous in luminous galaxies. On account of their low surface brightness, detailed study of their physical properties has been difficult and, until recently, confined largely to the Milky Way (MW) and Andromeda (M31). Since the advent of large cameras and surveys, both from ground and space, our knowledge of stellar halos has increased. For several late- and early-type galaxies, astronomers were able to measure the physical properties of their stellar halos out to hundreds of kiloparsecs, or beyond, revealing very low luminosity extended stellar structures, similar to the halos of the MW and its closest neighbouring spiral M31.

Observations show that these halos have complex morphologies with multiple stellar components, complex kinematics and substructures that indicate a history of merger and accretion events. These morphologies resemble the density maps from cosmological simulations of galaxy formation in a hierarchical Universe. Consequently a large amount of effort has been invested in trying to understand how we go from a qualitative resemblance to quantitative measurements of the fractions and frequencies of these substructures.



Figure 1. Participants of the Stellar Halos 2015 workshop in front of the ESO Headquarters building.

The Stellar Halos 2015 workshop brought together around 90 observers and theorists (see Figure 1), who discussed results from space- and ground-based surveys of stellar halos in late- and early-type galaxies and their comparison with the predictions from cosmological simulations. All the presentations were collected and are now posted on the workshop web page¹, under Programme. A short, non-exhaustive, summary of the highlights is presented here.

What is a galaxy stellar halo?

Guinevere Kauffmann and Annette Ferguson set the stage for the workshop by addressing the question of what a galaxy stellar halo is from theoretical and observational perspectives. Kauffmann described the two main techniques for the theoretical studies of stellar halos: hybrid methods and full hydrodynamical simulations. According to the hierarchical cosmological model of Lambda Cold Dark Matter (Λ CDM), the Milky Way and other large galaxies of similar luminosity should have accreted and subsequently tidally destroyed ~ 200 low-mass galaxies in the past ~ 12 Gyr. The simulated stellar halo images produced by hybrid semi-analytic plus N-body models, such as those shown in Figure 2, from Bullock & Johnston (2005), display the complex structure of the halos as well as long-lived low surface brightness streams. Simula-

tions can now trace the build-up of stellar halos and the evolution of their properties. For example, the projected phase-space diagrams and plots of the line-of-sight velocity vs. radial distance relative to the host halo centre, can be used to identify the recent satellite disruption events both in simulations and in data (e.g., the talk by Alessia Longobardi on the extended substructure in the M87 halo — see also Longobardi et al., 2015).

However, not all halo stars are accreted. A fraction of the halo may be formed *in situ*, either by heating the disc stars to halo orbits, or by forming stars in the halo from in-falling gas. The in-falling gas may be stripped from sub-halos that merge with the host galaxy, or enter through direct infall. This dichotomy of “*in situ*” vs. “accreted” halos has led to discussions about the dual halo nature that was emphasised by Annalisa Pillepich, who showed results from a new set of simulations called Illustris. Andrew Cooper showed the power of the particle tagging method in making detailed predictions for the statistical properties of stellar halos that directly link CDM structure formation to photometric and spectroscopic halo observations.

Simulated images of stellar halos, like the one shown in Figure 2, can be compared with the observed surface brightness maps around nearby galaxies. Observationally, halos can be studied by stacking images of similarly bright objects, yielding deep photometry of integrated light, and by directly detecting individual stars and

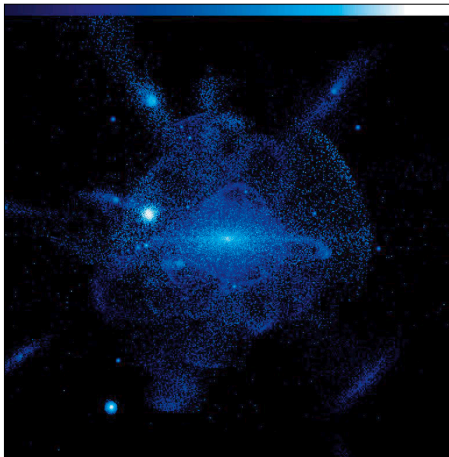


Figure 2. A simulated stellar halo surface brightness image² shown with a cut at 40 mag arcsec⁻² (image from Bullock et al., 2005).

other tracers. Yet, Annette Ferguson emphasised that in order to measure substructures in stellar halos, accurate surface brightness photometry down to $\mu_v \sim 30$ mag arcsec⁻², i.e., ~ 9 – 10 mag (0.05 %) below the surface brightness of the dark night sky, on angular scales equivalent to ~ 100 – 200 kpc around MW-sized galaxies, is required. This is observationally very challenging! Since different assembly histories for galaxies may lead to complex, heterogeneous and evolving structures, galaxy samples made up of a range of morphological types and environments are also necessary.

Stellar halos of the Milky Way and Andromeda

The Milky Way and Andromeda are the two nearest large galaxies whose halos are being extensively studied. In his review of the Milky Way stellar halo, Wyn Evans quoted the fundamental observation from Eggen, Lynden-Bell and Sandage (1962): “The time required for stars in the halo to exchange their energies and angular momenta is very long compared with the age of the Galaxy. Hence, knowledge of their present energy and angular momenta tells us something of the initial conditions under which they formed.” Such a statement, which is more than half a century old, illustrates very clearly the motivation for studying the dynamics of streams in galaxy halos. For example, the disrupted

Sagittarius dwarf provides ~ 20 % of all the debris of the stellar halo in the Milky Way, including multiple extended stellar streams and of the order of 20 globular clusters. The modelling of this stream constrains the Galaxy potential and its associated mass to ~ 5 – $8 \times 10^{11} M_\odot$ within 200 kpc, in agreement with the kinematics of halo stars and satellites in the Local Group.

Paula Jofre reported on measurement of the ages of individual stars in the MW halo, demonstrating that they are very old, having been formed 10–12 Gyr ago. The more metal-rich component tends to have a higher fraction of younger stars. There is also a bifurcation in the age–metallicity relation seen in stellar clusters and in field stars at $[\text{Fe}/\text{H}] = -1.4$ dex. Giuseppe Bono presented a study of the Galactic Halo metallicity gradient based on a homogeneous set of RR Lyrae stars with accurate distances. The RR Lyrae stars are particularly suitable tracers of the old Galactic Halo, showing a linear shallow metallicity gradient. The younger *in situ* component however is not traced by RR Lyrae stars, which are all at least 10 Gyr old. Future spectroscopic surveys of RR Lyrae stars will also enable comparison with simulations that predict different kinematical signatures for the *in situ* vs. accreted components.

Two large surveys have investigated the stellar halo of M31: the Pan-Andromeda Archeological Survey (PAndAS) and the Spectroscopic and Photometric Landscape of Andromeda’s Stellar Halo (SPLASH). The PAndAS results, presented by Rodrigo Ibata, are based on a detailed photometric map extending beyond the 150 kpc radius around M31 and covering also M33, using the Canada-France-Hawaii Telescope (CFHT). The metal-poor halo of Andromeda is found to be smoother than the metal-rich part. Numerous dwarf galaxies and globular clusters as well as streams without clear progenitors, contribute to the network of rich substructure in the halo. Nicolas Martin, from the PAndAS survey, is comparing the Andromeda field of streams to Aquarius simulations, treating the observational and model datasets in a consistent way in order to reconstruct the assembly history of the halo.

Karoline Gilbert presented the SPLASH survey, which has traced the surface brightness profile out to ~ 180 kpc, finding a similar density profile to the PAndAS survey. The spectroscopic identification of more than 1500 M31 halo stars in the SPLASH survey has resulted in determination of the metallicity gradient out to large radii. The stellar density and metallicity profiles indicate that the M31 halo was largely built from one, or a few, relatively massive ($> 10^9 M_\odot$) accretion events, but at large radii many low-mass accretions have contributed to the recent build-up of the halo. The kinematics of the inner halo stars is however consistent with their origin from the disc — these stars were likely kicked out in a collision with a system similar in size to the Large Magellanic Cloud that collided with M31 ~ 760 Myr ago. The MW and M31 metallicity and α -element abundance gradients provide datasets that can be used as constraints to the simulations, such as those presented, for example, by Andreea Font.

Stellar halos in galaxies beyond the Local Group

Laura Greggio reviewed the current observational limitations and future opportunities for the studies of stellar halos. She made the case that resolved stellar population studies (single star photometry) should reach well below the red giant branch tip, hence arguing for deep observations. The shapes of the substructures and surface density profiles can then be used to assess the fraction of accreted halo stars and recover the individual galaxy accretion history. The European Extremely Large Telescope (E-ELT) and the James Webb Space Telescope (JWST) will open up the study of resolved stellar halos to ~ 30 Mpc distance, such as red giant stars in the halos of elliptical galaxies in Virgo. This advance will enable detailed studies of a statistically representative sample of large galaxies, and will connect the resolved stellar population to the integrated light studies.

Roelof de Jong and Antonella Monachesi presented detailed physical properties of individual galaxy halos beyond the Local Group for the spiral galaxies in the Hubble Space Telescope GHOSTS (Galaxy Halos

Outer disks Substructure Thick disks Star clusters) survey. The high angular resolution of the Hubble Space Telescope (HST) allows the detection of single stars in halos at larger distances and in denser regions — hence investigating the transition regions between the disc and halo. All MW-like galaxies observed by GHOSTS have extended stellar halos. Their power law profiles have a slope between $-2 < \alpha < -4.5$ over 10–70 kpc. The larger galaxies have fractionally larger envelopes and the inner halos are compact, with Sersic index $n \sim 5$, and are flat ($c/a \sim 0.3$).

Only a half dozen luminous early-type galaxies are close enough to resolve individual stars in the halos and study their properties. Marina Rejkuba summarised the previous studies, most of which concentrated on the nearest giant elliptical galaxy NGC 5128, known also as Centaurus A. The bulk of the stars in the halo of NGC 5128 formed at redshift $z > 2$, and these stars had very fast chemical enrichment, already reaching super-solar metallicity ~ 12 Gyr ago. This is the only early-type galaxy in which metallicity and stellar density gradients have been mapped to 25 effective radii, or 140 kpc distance. The halo appears to be elongated with a shallow metallicity gradient and some field-to-field variation in stellar density and metallicity, indicative of possible accretion events. This is not too surprising, since this galaxy is a known merger remnant.

On the other hand NGC 3379, a giant elliptical in the Leo group, has little or no indication of being disturbed or having recently accreted stars in its halo. Beyond ~ 12 effective radii in this galaxy there is a break in the metallicity distribution and the metal-poor component, which is typically associated with halos, starts to dominate. Mark Peacock presented the results from his HST study of NGC 3115, where there is also quite a high mean metallicity, extending to very large distances in the halo: the metallicity decreases from -0.65 to -0.8 dex between 15–60 kpc (6–23 effective radii). However, a distinct metal-poor population is identified in the two outer fields and its profile is found to trace the density profile of the metal-poor globular clusters. The metal-poor halo population mass fraction is $\sim 14\%$ of the total halo mass in NGC 3115.

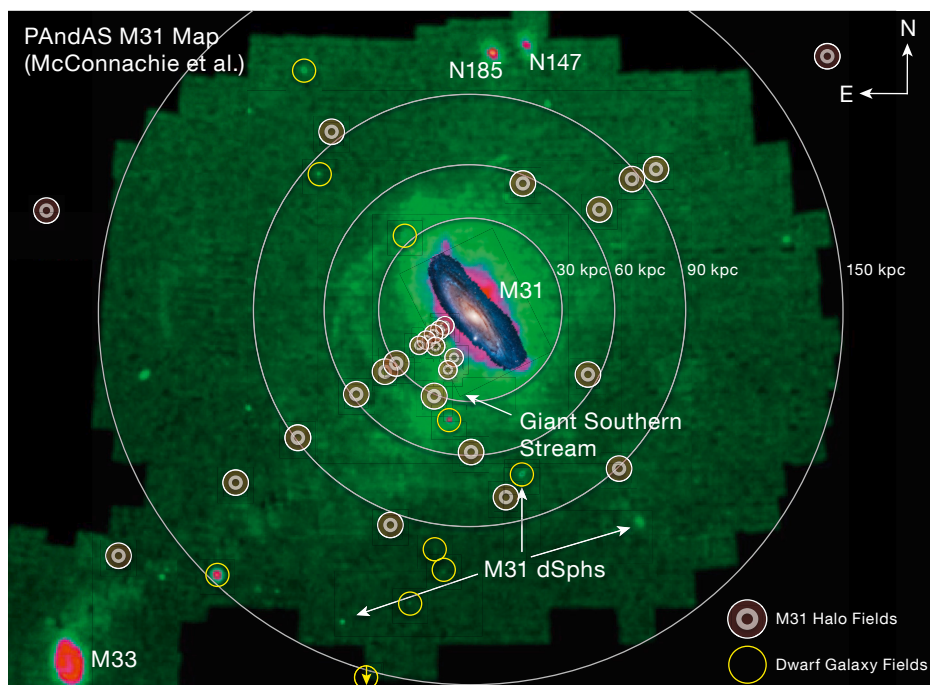


Figure 3. Map of the stellar counts in the Andromeda galaxy M31 from the PAndAS survey (McConnachie et al., 2009) with overlaid spectroscopic observation target fields from the SPLASH survey³.

More distant early-type galaxies, in the Virgo and Fornax clusters, have too high a density of stars for accurate resolved stellar population studies, hence deep surface brightness observations are favoured for the study of their faint envelopes. Chris Mihos has traced the envelope of M49 at the centre of the Virgo sub-cluster B out to ~ 150 kpc. A steep bluer colour gradient has been measured in the outer regions indicating a very high fraction of metal-poor stars in its outskirts. Enrichetta Iodice and Marilena Spavone examined the extended envelopes of individual Virgo and Fornax cluster galaxies from VLT Survey Telescope and OmegaCAM guaranteed time observation programmes. The CFHT was used by Pierre-Alain Duc to systematically survey the extended regions around galaxies whose internal kinematics and stellar populations were observed by the ATLAS^{3D} project. Several instrumental effects may limit the accuracy of these measurements: flat-fielding, scattered light, corrections due to the wings of the point spread function and halos due to internal reflections in the camera, as well as Galactic cirrus, must be taken into account.

Nevertheless tremendous progress has been achieved and there are ever-larger samples of galaxies where faint halos and streams are detected.

Particularly impressive accretion streams were presented by David Martinez-Delgado, based on imaging with small (0.1–0.5 metre) robotic telescopes. These observations reveal structures around galaxies with a striking resemblance to those shown by cosmological simulations of structure formation. Richard D’Souza presented the statistical properties of stellar halos. By carefully stacking a very large number of galaxies, he found that the stellar halos of late-type galaxies tend to be spherical, while those of early-type galaxies tend to be elliptical. The ellipticity increases with stellar mass, and also the fraction of light in the outskirts is higher in the more massive galaxies. The surface density profiles agree with the results from simulations using particle-tagging methods.

Magda Arnaboldi, Pat Durrell and Jean Brodie presented the use of discrete tracers, like planetary nebulae and globular clusters, to study the physical properties of the extended halos. Durrell and Brodie illustrated how red and blue globular clusters trace different components in the halos. The red globular

cluster populations have number density profiles similar to that of the stars, while the blue globular clusters are spatially more extended and seem to trace the metal-poor halo component. Arnaboldi showed the overlap of the M87 halo and the intracluster light in the radial range between 20 to 150 kpc from the centre of M87, and how the planetary nebulae luminosity function is used to identify the star-forming (metal-poor) stellar population vs. the old and metal-rich one. Michael Hilker showed that there are different sub-populations of globular clusters in the distant central galaxy in the Hydra cluster that trace different assembly epochs. The origin of ultra-compact dwarfs around NGC 1399, the central galaxy of the Fornax cluster was presented by Karina Voggel. Ortwin Gerhard, Nicola Napolitano and Eric Emsellem described the kinematics of stars, their angular momentum and orbital distribution in galaxies from the centre out to ten effective radii.

While the stellar mass is a strongly non-linear function of the galaxy halo mass, due to the large contribution of dark

matter in the least and the most massive galaxies, the total mass of all globular clusters correlates linearly with the mass of the halo, as shown by Bill Harris. This is explained if globular cluster formation is largely immune to the feedback that affects star formation in the field, or if the formation of globular clusters is completed before the feedback starts.

Prospects

During the final discussion, the obvious energy and enthusiasm testified that this field of research had gained substantial momentum! The observational samples are growing and we are starting to make quantitative comparison of the properties of halos inferred by different observational techniques with the simulations. The importance of consistent comparisons was emphasised yet again: there are different ways to define a stellar halo — including or excluding the streams and accreted material — which then lead to different halo properties. Hence the halo properties need to be

studied in a homogeneous and unbiased way, by applying a consistent treatment to observations and theory/simulations. Lively discussions during the workshop, after every talk, during coffee breaks, and the vibrant atmosphere during the final gathering around *Bier und Bretz'n*, resulted in new ideas, new collaborations and projects for future advances in the field.

References

- Bullock, J. S. & Johnston, K. V. 2005, *ApJ*, 635, 931
 Eggen, O. J., Lynden-Bell, D. & Sandage, A. R. 1962, *ApJ*, 136, 748
 Longobardi, A. et al. 2015, *A&A*, in press, arXiv:1504.04369
 McConnachie, A. W. et al. 2009, *Nature*, 461, 66

Links

- ¹ Workshop programme: <http://www.eso.org/sci/meetings/2015/StellarHalos2015/program.html>
² Image of simulated stellar halo: <http://www.physics.uci.edu/~bullock/StellarHalo/halo.html>
³ Annotated image of M31: <https://blogs.stsci.edu/universe/2014/07/21/what-built-andromedas-stellar-halo/>

Report on the ESO Workshop

Dissecting Galaxies Near and Far

held at ESO Vitacura, Santiago, Chile, 23–27 March 2015

Catherine Vlahakis^{1,2}

¹ Joint ALMA Observatory, Santiago, Chile

² ESO

The workshop explored high-resolution perspectives for the understanding of star formation and the interstellar medium in the era of ALMA. Angular and spectral resolutions are fundamental limitations for our understanding of the properties of galaxies in the nearby and distant Universe. A new generation of instruments and powerful observatories, as well as planned future facili-

ties, is pushing out the boundaries of what was previously possible over the entire electromagnetic spectrum. Held in the approach to ALMA Early Science Cycle 3, the workshop centred on discussing the scientific results and upcoming opportunities afforded by the new capabilities available in the era of ALMA. Some of the science highlights of the meeting are presented.

The advent of state-of-the-art facilities with high angular resolution and/or high spectral resolution capabilities, coupled with high sensitivity, such as the Atacama Large Millimeter/submillimeter Array (ALMA), allows the interstellar medium

(ISM) and star formation properties of galaxies at intermediate redshift to be probed in unprecedented detail, along with their counterparts in the local Universe.

The aim of the workshop was to bring together astronomers whose interests further our understanding of star formation and ISM processes at high spatial and spectral resolution, both in nearby and distant galaxies. The theme of “dissecting galaxies” was intended not only to encompass what we can learn by going to higher spatial and spectral resolution, but also, in the true sense of the word “dissect”, what we can learn about galaxies when we methodically break them down into their constituent

components. Workshop topics included: the high-redshift Universe, ISM, star formation and environment, star formation, the star formation–molecular gas connection, the nuclei of galaxies, nearby galaxies, and galaxy groups and clusters.

Emphasis on synergies between current and future facilities capable of carrying out such observations, and synergies with ALMA in particular, were encouraged. Participants discussed recent scientific results and future opportunities using a wide range of telescopes, including ALMA, the Hubble Space Telescope (HST), Herschel, Spitzer, the Wide-field Infrared Survey Explorer (WISE), Jansky Very Large Array (JVLA), the Very Large Telescope (VLT), Combined Array for Research in Millimeter-wave Astronomy (CARMA), the South Pole Telescope, the Atacama Pathfinder EXperiment (APEX), Australia Telescope Compact Array (ATCA), Institut de Radioastronomie Millimétrique (IRAM), Plateau de Bure Interferometer (PdBI), the Northern Extended Millimeter Array (NOEMA), the James Webb Space Telescope (JWST), the Square Kilometer Array (SKA), and many more besides. The workshop aimed to be scientifically rich, but also informal, with ample time for less formal discussions and social activities (Figure 1). Here, we provide a summary of some of the highlights of the meeting. The workshop programme and presentations are available for download¹.

Molecular gas and star formation in the Galaxy and nearby galaxies

Most stars form in giant molecular clouds (GMCs), and the relationships between molecular gas and star formation are a key issue for understanding galaxy evolution. High spatial resolution observations of the Magellanic Clouds and nearby galaxies may provide an important bridge between the properties of Galactic GMCs and distant galaxies. The evolution of GMCs in the Large Magellanic Cloud (LMC) was presented in a review by Toshikazu Onishi. From ALMA observations, he showed a wealth of filaments and arcs (Fukui et al., 2015; see Figure 2) and molecular outflows, with some filaments colliding and leading to rapid high-mass star formation. Monica Rubio pre-



Figure 1. The workshop participants photographed during the workshop dinner held in the ESO Vitacura gardens.

sented results on the Magellanic Bridge, in which she discussed the problems of searching for dark molecular gas in low-metallicity environments and showed the presence of a submillimetre dust excess.

On the topic of nearby galaxies, Sharon Meidt presented results from PdBI observations of the nearby spiral galaxy M51 (e.g., Meidt et al., 2013) showing the role of spiral arms on gas organisation and star formation. She showed that molecular clouds are sensitive to environment and respond to local conditions, and that

spiral arms affect the structure and organisation of the ISM down to cloud-scales.

Star formation laws

Adam Leroy presented a review of the physical conditions in the ISM and star formation. The relationship between molecular gas and recent star formation (“star formation law”; SFL) in local galaxy discs shows physically driven variations when the data is dissected, whether into different galaxy types or different galaxy regions — such as whole discs, kpc-sized regions, galaxy centres and starbursts (Leroy et al., 2013; see Figure 3,

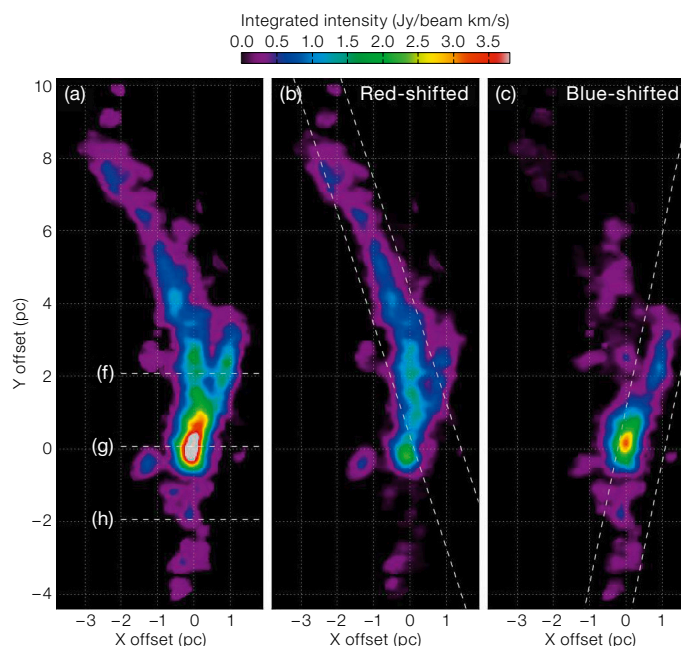


Figure 2. ALMA ^{13}CO (2-1) integrated intensity images of filaments detected in the LMC (N159), produced for different velocity ranges. Left panel: Full velocity range; centre and right panels: red-shifted and blue-shifted velocity ranges. From Fukui et al. (2015).

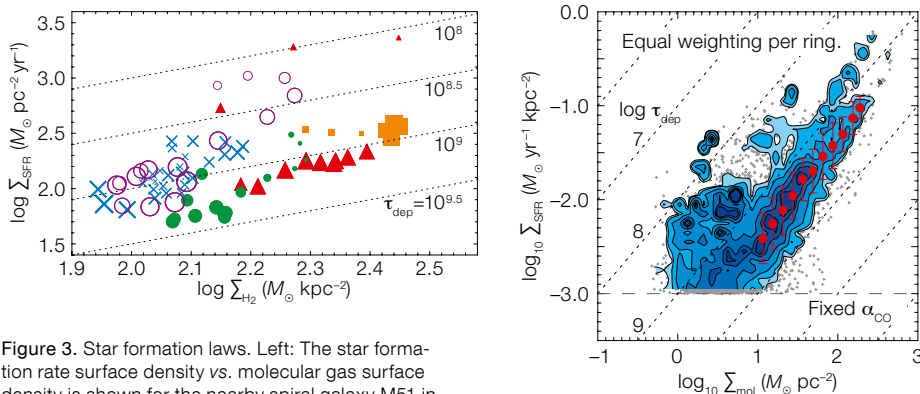


Figure 3. Star formation laws. Left: The star formation rate surface density vs. molecular gas surface density is shown for the nearby spiral galaxy M51 in different radial bins. From Meidt et al. (2013); data from the IRAM PdBI. Right: The star formation law for a sample of 30 nearby disc galaxies at 1 kpc resolution; low- z dwarf galaxies, starbursts and large disc galaxies occupy different regions of the plot. From Leroy et al. (2013); data from the IRAM 30-metre telescope.

right). He also presented plans to study dense gas and star formation in normal galaxies, via surveys of HCN, with ALMA and other facilities. The SFL and its connection between molecular gas and star formation was discussed by several other speakers, including: Linda Watson, who showed that a similar relationship applies to extended ultraviolet disc galaxies as within optical discs; Sharon Meidt, who showed the relationship for M51 (Meidt et al., 2013; see Figure 3, left); and Chelsea Sharon, who discussed problems for understanding the SFL at high redshift.

Galactic nuclei

In a three-part review on the theory, observations, dynamics and chemistry of galactic nuclei, Francoise Combes started by reviewing theoretical perspectives on molecular outflows from active galactic nuclei (AGN) and AGN feedback. Then Santiago Garcia-Burillo reviewed the observational perspectives. He showed results from the IRAM 30-metre, PdBI, NOEMA and ALMA telescopes to show how large-scale bars and interactions drive gas inflow down to 0.1–1 kpc scales, and he presented mounting evidence for molecular winds in starbursts, local AGN, radio galaxies and ultraluminous infrared galaxies (ULIRGs). Susanne Aalto focused on the physical conditions and chemistry of the hot cores and cold outflows, in particular using recent ALMA

results. She showed the impressive chemical richness revealed in AGN and starburst nuclei and a wealth of molecular outflows, including an intriguing jet-like outflow in NGC 1377 that appears to flip directions (Aalto et al., in prep.).

Galaxy groups and clusters

The effect of environment on ISM properties, and in particular ram-pressure stripping (RPS), was discussed in a session dedicated to galaxy groups and clusters. Jeff Kenney presented clear evidence of strong RPS in NGC 4921, the most massive spiral galaxy in the Coma Cluster, with impressive Hubble Space Telescope imaging at 30 pc resolution showing a dust front of swept-up gas and dust along the leading edge of ram-pressure interaction (Kenney et al. [2015] submitted). Ram-pressure stripping can completely strip the ISM in massive galaxies in Coma-like clusters. Kenney showed evidence for dense cloud decoupling and magnetic binding in the ISM. The effect of RPS on the intra-cluster light (consisting of both gas and stars) at $z \sim 0.5$ was presented by Emanuela Pompei for the cluster XLSSC 116, using observations that included MUSE Science Verification data.

Early-type galaxies contain ISM

While much of the discussion on nearby galaxies focused on spiral galaxies, Martin Bureau reviewed what we know about the molecular gas content of early-type galaxies, once thought to be devoid of ISM. He described CARMA CO obser-

vations (Alatalo et al., 2013; Davis et al., 2013) that show CO structures in early-type galaxies ranging from discs to rings to bars and how the kinematic misalignment gives insight into the origin of the gas. He showed that CARMA CO imaging of NGC 4526 (Davis et al., 2013, Utomo et al., 2015; Figure 4) at 20 pc resolution (i.e., molecular cloud scale) exhibits regular disc kinematics. This allows strong constraints to be placed on the supermassive black hole mass, leading to promising plans to measure supermassive black hole masses using CARMA/ALMA molecular gas observations.

The high-redshift Universe

Jacqueline Hodge presented a review of galaxies at high redshift from a molecular line perspective, describing recent progress in our understanding of molecular gas in high- z galaxies through targeted observations of far-infrared bright and colour-selected sources and also blind deep fields. Rob Ivison reviewed our understanding of galaxies at high redshift from a submillimetre continuum perspective. Both described how the high angular resolution of ALMA, combined with high sensitivity, allows the rapid mapping of large numbers of single-dish detected submillimetre galaxy sources, providing unambiguous counterparts when combined with optical spectroscopy or redshifts determined with ALMA via blind line scans (e.g., Spilker et al., 2014; see Figure 5, upper).

Gravitational lensing as an essential probe of high- z galaxies down to scales of less than a few hundred parsecs, using ALMA and JVLA, was discussed by several speakers, including Kirsten Knudsen, Alasdair Thompson, Manuel Aravena, Chelsea Sharon and Jacqueline Hodge. Results presented included the very high angular resolution submillimetre observations now possible with ALMA's long baseline capability that probe to sub-kpc scales at $z \sim 3$ in a gravitationally lensed system (ALMA Partnership, Vlahakis et al., 2015; see Figure 5, lower).

Making $z = 2$ – 5 seem like the local Universe, Brant Robertson presented a review of early galaxy formation and evolution through the eyes of new facilities,

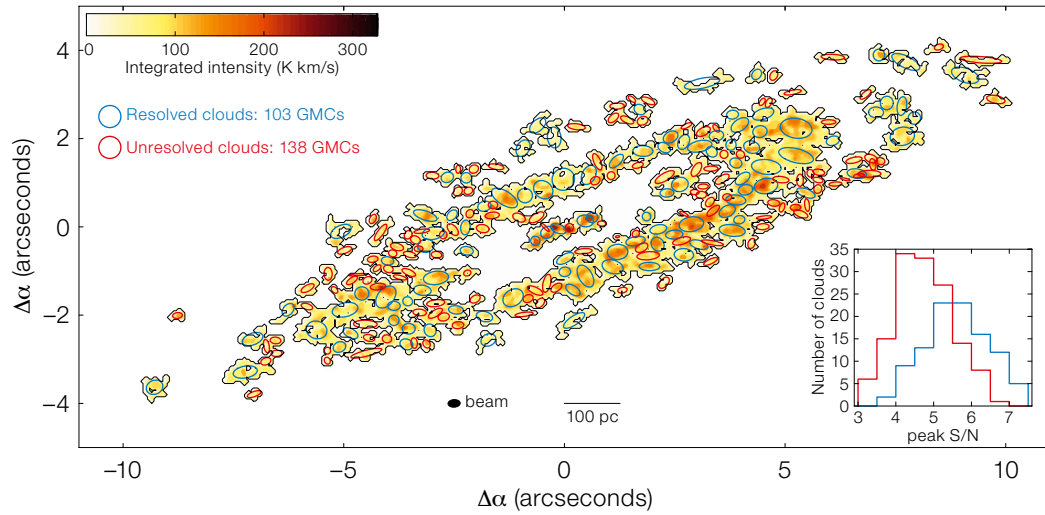


Figure 4. CARMA CO J=2-1 integrated intensity image of the early-type galaxy NGC 4526 from Utomo et al. (2015) at 20 pc spatial resolution; circles indicate giant molecular clouds (GMCs).

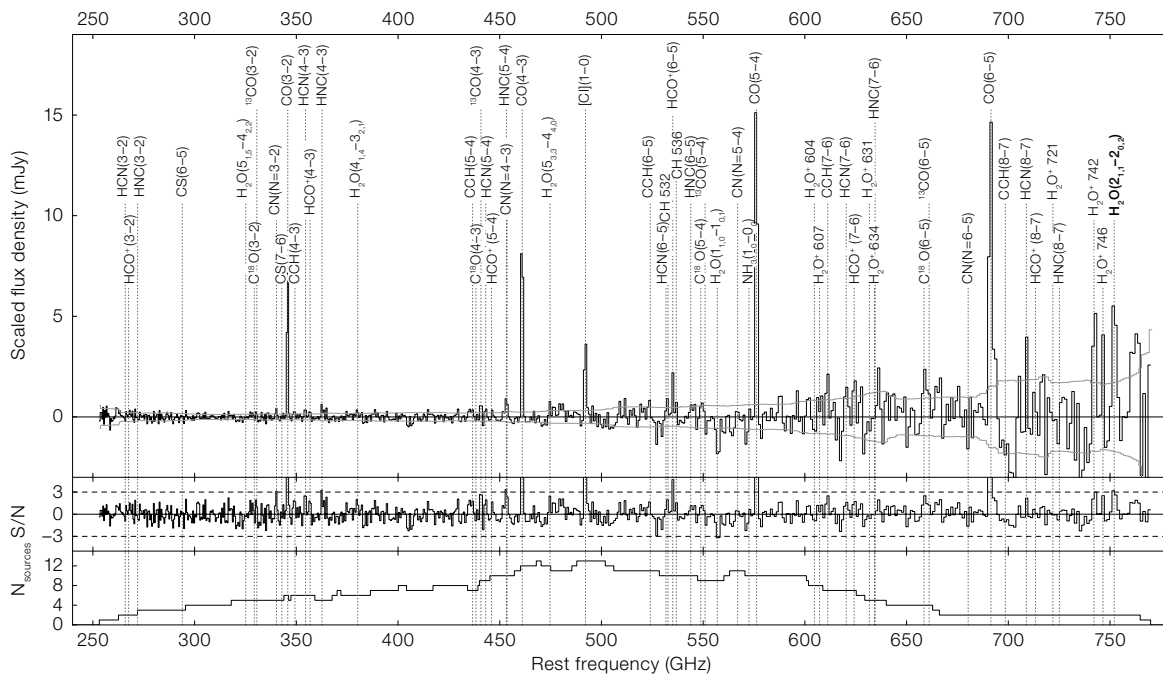
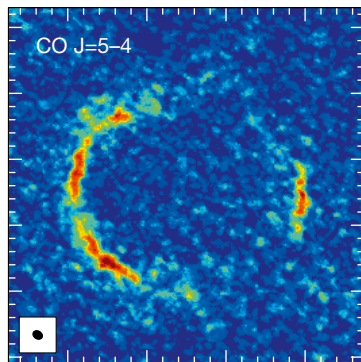
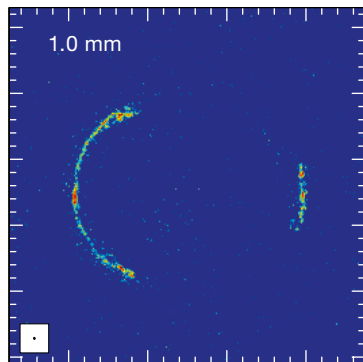


Figure 5. Examples of ALMA's powerful spectral (upper) and spatial (lower) capabilities. Upper: Composite spectra for a sample of 22 dusty starburst galaxies, showing potentially detectable molecular lines. From Spilker et al. (2014). Lower: The lensed galaxy H-ATLAS J090311.6+003906 imaged in 1 mm continuum at 31×23 mas resolution, and CO J=5-4 at ~ 170 mas. From ALMA Partnership, Vlahakis et al. (2015). When combined with high sensitivity, such observations open up a new frontier for the study of high-redshift gravitationally lensed galaxies.



focusing on the theoretical perspective. He reported on the new population of high-redshift galaxies discovered out to $z \sim 10$, what they can tell us about the role of galaxies in reionisation, and the uncertainties about the properties of high-redshift galaxies, including the production rate of ionising photons and the fraction that escape to ionise the intergalactic medium. In particular he described the strong ultraviolet-optical line emission that will in future be confirmed with JWST, and how the powerful

combination of ALMA and JWST will teach us about the ISM conditions and stellar populations of high-redshift galaxies.

Prospects

The workshop was timed to coincide with the ALMA Cycle 3 Call for Proposals, which, for the first time, offered the high angular resolution capability. At the end of the workshop there was a presentation on ALMA Cycle 3 capabilities, and discussion groups were formed to discuss possible ALMA proposals. A visit to the ALMA site at Chajnantor was also organised.

The rich variety of science presented at the meeting, covering topics ranging

from our Galaxy to galaxies at redshift 10, highlighted the impressive scientific promise of ALMA and contemporary instruments for producing high resolution, high impact results in the coming years.

Acknowledgements

Thanks go to the other members of the Scientific Organising Committee: Rebeca Aladro, Manuel Aravena, Guillermo Blanc, Alberto Bolatto, Daniela Calzetti, Pierre Cox, Dimitri Gadotti, Daisuke Iono, Kotaro Kohno, Mark Krumholz, Sergio Martin-Ruiz, Juan Carlos Munos-Mateos, Nick Scoville, Jonathan Tan, Jean Turner, Baltasar Vila Vilaro and Christine Wilson. The Local Organising Committee: Rebeca Aladro, Daniel Espada, Maria Eugenia Gómez, George Hau, Paulina Jirón, Evelyn Johnston, Juan Carlos Munos-Mateos and Linda Watson is warmly thanked. Both committees facilitated an exciting workshop programme with a relaxed, yet full and diverse schedule, including many opportunities for

informal, but lively discussions, and enjoyable social activities. Special thanks go to Pierre Cox, ALMA Director, for presenting the workshop summary, and to Maria Eugenia Gómez and Paulina Jirón for their patient and efficient help with all the practical aspects of organising this meeting.

References

Alatalo, K. et al. 2013, MNRAS, 432, 1796
ALMA Partnership, Vlahakis, C. et al. 2015, ApJL, in press, arXiv:1504.04877
Davis, T. et al. 2013, MNRAS, 429, 534
Fukui, Y. et al. ApJL, submitted, arXiv:1503.03540
Leroy, A. et al. 2013, ApJ, 146, 19
Meidt, S. et al. 2013, ApJ, 779, 45
Spilker, J. S. et al. 2014, ApJ, 785, 149
Utomo, D. et al. 2015, ApJ, 803, 16

Links

¹ Workshop programme: <http://www.eso.org/sci/meetings/2015/Galaxies2015/program.html>

Report on the

ALMA/Herschel Archival Workshop

held at ESO Headquarters, Garching, Germany, 15–17 April 2015

Evanthia Hatziminaoglou¹
Martin Zwaan¹
Leonardo Testi¹

¹ ESO

The Herschel mission produced data from 2009 to 2013 and ALMA Cycle 0 began in 2012. The lower frequency Herschel capabilities overlap the higher frequency ALMA bands but, despite differences in spatial resolution, Herschel provides targets for ALMA follow-up. Following up on a previous Herschel ALMA archival workshop, this one provided a large number of comparative studies using both archives. An overview of the workshop is provided, covering topics from cosmology to the Solar System.

In late 2010, right in the middle of the Herschel science mission and ahead of



the start of ALMA Early Science, we organised a workshop at ESO Headquarters in Garching on the expected impact of the Herschel surveys on the science programmes being prepared for ALMA (reported in Testi et al., 2011). After three

Figure 1. Participants of the workshop in front of the ESO Headquarters building.

successful cycles of ALMA Early Science proposals and prior to the Cycle 3 deadline, it was time to organise a workshop

focused on the synergies of ALMA and Herschel joint archival research.

The Herschel Space Observatory has produced high quality photometric and spectroscopic data in the wavelength range of approximately 55–670 μm during its lifetime from 2009 to 2013. To date, all Herschel science data (~ 23 400 hours of observations, ~ 37 000 Astronomical Observation Requests [AORs]), in addition to a variety of user-provided data products, are publicly available through the Herschel Science Archive¹. Meanwhile, the ALMA Science Archive² is continuously being populated with observations that were carried out in the first three ALMA observing cycles, with more data becoming publically available by the day.

Motivation

The higher frequency ALMA bands overlap with the lower frequency (longer wavelength) Herschel bands, and despite the huge difference in spatial resolution, Herschel sources provide ideal targets for ALMA follow-up. Furthermore, with more and more ALMA data becoming publicly available, the possibilities for further exploration of these two complementary datasets are increasing immensely. However, Herschel and ALMA data differ greatly and in order to explore their full potential, archival users need to be aware not only of the contents of the two archives, but of the differences between the datasets as well, hence the need for such a workshop.

The target audience consisted of all astronomers who had already used data from either of the two facilities and would want to expand their knowledge to the neighbouring wavelength regime. The workshop focused on ALMA/Herschel synergies and archival research, with the following scope and goals:

- to provide examples of science cases based on the combined use of Herschel and ALMA data, covering a broad range of astrophysical topics, from star formation to evolved stars to galaxies and cosmology;
- to promote mutual awareness of the Herschel and ALMA data archive contents;
- to demonstrate how to explore, access

and visualise Herschel and ALMA data products; and

- to enable Herschel and ALMA archival science.

The workshop was divided into two parts: a technical first half day, where the ALMA and Herschel archives and their contents were described, followed by two full days of science talks, each split into two themes.

Four invited talks covered the major advances made jointly with ALMA and Herschel data in the most prominent fields of astrophysics (one per theme), namely the Universe at high redshift, galaxies at low redshift, star and planet formation processes and astrochemistry. The contributed talks and posters then focused on individual projects covering and expanding on the same topics, even touching upon observations of the Solar System. Among the many new results presented during the workshop, we briefly highlight a few interesting ones that illustrate the power of a combined Herschel and ALMA approach.

Extragalactic studies

Combined observations from ALMA and Herschel’s Spectral and Photometric Imaging Receiver (SPIRE) show submillimetre galaxies (SMGs) to have star formation rates of ~ 300–1000 $M_{\odot} \text{ yr}^{-1}$, substantial mass in stars (~ $6 \times 10^{10} M_{\odot}$) and cold molecular gas fractions of ~ 40 %, all properties that are expected for the progenitors of today’s massive spheroids and elliptical galaxies (presentation by Mark Swinbank). At the same time, ALMA follow-up of the GOODS-Herschel (Great Observatories Origins Deep Survey: far-infrared imaging with Herschel) detections of main sequence galaxies at $z = 3$ shows lower star formation rates in these galaxies than measured by Herschel, possibly indicating a change in the slope of the main sequence at those high redshifts, or, alternatively, that ALMA is over-resolving these galaxies (talk by Maurilio Pannella). Also dust and gas masses estimated from either Herschel or ALMA can be very different, and it was shown that only a combined ALMA–Herschel approach allows accurate gas and dust masses to be determined (Stefano Berta).

The brightest SMGs detected in the high-flux tail (> 100 mJy) of Herschel surveys, have turned out to be strongly lensed starburst galaxies at redshifts $z = 2$ –5. Following up these sources with ALMA, has resulted in spectacular images, such as the one of SDP.81, one of the Science Verification targets observed as part of the ALMA Long Baseline Campaign (see Vlahakis et al., p. 2). With ALMA’s unprecedented spatial resolution, the structure of the lensed galaxy can be reconstructed, resulting in continuum and gas maps with a spatial resolution of ~ 50 pc. These maps reveal both clumpy and diffuse star-forming regions (Matus Rybak).

The combination of Herschel data with ALMA observations is a powerful tool for characterising the physical conditions of the interstellar medium (ISM) in nearby galaxies (talk by Leslie Hunt). The combined approach allows us to study the mechanisms responsible for getting dust and gas in and out of galaxies, which eventually drives the evolution of galaxies. Herschel/SPIRE 870 μm observations of nearby galaxies have revealed a dust continuum excess compared to the predictions of standard dust models, and this excess increases toward lower-mass galaxies. With the much higher spatial resolution observations of ALMA, a physical connection between the dust properties and their exact sites can be drawn (Maud Galametz).

From the Galactic ISM to the Solar System

The rich chemistry of the Galactic interstellar medium can also be effectively studied by combining ALMA and Herschel data. Herschel reveals the large-scale structure of the ISM and has enabled the study of molecular species mostly out of reach from the ground, such as water. ALMA offers the sensitivity and angular resolution to study the inner structure of cloud cores and to probe the growth of chemical complexity, possibly leading to pre-biotic molecules (Paola Caselli). High angular resolution follow-up with ALMA of an infrared dark cloud, detected by Herschel, shows a surprising lack of a distributed low-mass protostellar population in the clump. The indications are that in a protocluster, low-mass stars form at a later stage after the birth of more

massive protostars (Ke Wang). The combination of high excitation molecular lines observed by Herschel and the low excitation lines observable with ALMA allow the role of turbulence in dense molecular clouds to be constrained (Andy Pon).

Herschel observations of protoplanetary discs have allowed us to expand our knowledge of the different evolutionary phases of discs, as initially defined by Spitzer surveys. The far-infrared photometric observations alone are not able to fully constrain the disc structure and evolution, but the Herschel catalogues provide excellent databases for extracting interesting sources for ALMA follow-up (presentations by Alvaro Ribas Gómez and Hector Canovas).

Several presentations focused on the prototypical carbon-rich evolved star IRC+10216, repeatedly observed by both ALMA and Herschel, with surprising out-

comes, such as the detection of hydrides or CH₃CN, and even a suspicion of the existence of a toroidal structure around the star (Guillermo Quintana-Lacaci, Luis Velilla Prieto and Marcelino Agundez). The detailed mechanism of molecule formation and evolution in the expanding shells around the star of IRC+10216 can only be traced through extensive and spatially resolved spectral line surveys, complemented by laboratory measurements and models (José Cernicharo).

Finally, observations of the atmosphere of Titan with Herschel and ALMA were also presented. These data, in combination with detailed atmosphere models, allow the chemistry of the satellite and the possible evolution of its atmosphere to be constrained. Future ALMA observations will allow the search for more complex and less abundant molecules and to resolve the vertical structure of Titan's atmosphere (Miriam Rengel).

Other than the astounding scientific results, the main outcomes of the workshop were that synergies between the Herschel and the ALMA data and archives will continue to exist long after the end of Herschel operations, and that both facilities will leave a great legacy behind, thanks to their respective archives.

References

Testi, L., Pilbratt, G. & Andreani, P. 2011, *The Messenger*, 143, 52

Links

¹ Herschel Science Archive: <http://www.cosmos.esa.int/web/herschel/science-archive>

² ALMA Science Archive: <http://almascience.eso.org/aq/>

Fellows at ESO

Joe Anderson

I grew up in the countryside near Carlisle, a small city in the north of England very close to the border with Scotland. As over all of the UK, the skies were dominated by clouds and rain; however during those few clear nights, beautiful star-filled skies could be seen due to the relatively low level of light pollution. In addition, our family used to take a yearly holiday to the west coast of Scotland in a remote village called Glenelg. Many a night was spent around fires on the beach below the stars. While I think that these experiences may have influenced my later life/career choices, at that stage I never thought that I would have a career as a professional astronomer.

At secondary school I excelled at maths and physics, and hence chose to study those (together with chemistry) as A-levels

(16–18 year education). When university degree decision time came, I was slightly lost in terms of the direction for my continued education/career. The obvious choice was to continue and study physics further, but the exact details were not clear. In the end I chose to do a physics with astronomy course at the University of Liverpool/Liverpool John Moores University. However my parents still joke that this was simply because “Astronomy” is one of the first courses to appear in university prospectuses!

While I enjoyed the content of many undergraduate courses, it was only when I started my first research project that I really began to feel motivated to push myself further. This first research project introduced me to the topic of supernovae, and formed the basis of my research to complete my MPhys degree. At the same time we were invited to attend



Joe Anderson

seminars at the Astrophysics Research Institute (ARI, Liverpool John Moores University [LJMU]), together with journal

clubs and other general research activities. At this point I saw a clear shift in the learning experience. Whereas previously in school, and at early undergraduate level, it seemed as if the emphasis was on gaining specific knowledge/skills as defined by teachers/lecturers, now the emphasis was almost completely on the student to drive the direction of study/research. Being allowed/encouraged to basically do what one wants motivated me to continue to do research and still motivates me to continue today, where freedom to continue research in the direction of one's personal interests makes the academic research life such an enjoyable one. Hence, the next natural progression was to continue to study for a PhD, for which I stayed in Liverpool and continued the subject of my MPhys research as my thesis topic at the ARI, LJMU. My thesis concentrated on constraining the progenitor characteristics of supernovae through studying their parent stellar populations within host galaxies. Indeed, this is a subject on which I continue to spend significant research time to this day.

After completing my PhD in 2009, I moved to Chile to start a postdoc position at the Universidad de Chile. Chile has long been an important player in the supernova research community, and this position gave me the opportunity to collaborate with many supernova experts. After two years as a postdoc, I was awarded a FONDECYT fellowship (Chilean national research fellowship), and continued my stay at Universidad de Chile for another three years. During this time I also became a father for the first time (we now have a second child) with my Chilean girlfriend, and hence my ties to Chile became stronger. Being awarded an ESO Fellowship enabled me to continue both my family and research life in Chile, while giving me the opportunity to work at the Paranal Observatory.

I very much enjoy my shifts at Paranal, in particular the interaction with non-astronomers which gives one a different perspective to the world of astronomy. Being at the end point of science operations also enables insight into the exact workings of instruments and the intricacies involved in performing the most efficient observations. Indeed, this experience has driven a new project: The All-

weather MUse Supernova Integral field Nearby Galaxies (AMUSING) survey, for which I am the PI. This project uses sub-optimal observing conditions to observe supernova host galaxies with the recently commissioned MUSE instrument, with the aims of constraining supernova progenitors, refining the use of supernovae to understand the Universe, and furthering knowledge of galaxy evolution, dynamics and stellar populations. The survey is rekindling my studies on supernova environments, the first field that persuaded me to follow a career in astronomy.

A recurring theme that one encounters as a professional astronomer is the question of spending public money on blue-skies research. This question can be particularly pertinent in Chile/South America, where many people still live in significant poverty, and it is something I am continually debating with non-astronomy Chilean friends and family. There are many standard answers to such a question, many of which concentrate on examples of subsequent benefits to society. However, my opinion (and one that I stress in all such discussions) is simply that this funding is justified because as human beings we always want to know why. From a young child seeing stars on a clear cold night to professional astronomers directing a state-of-the-art telescope at a galaxy far from the Earth, our interest is driven by the question of why. To me this simple fact is sufficient to justify astronomy research and I am honoured to be able to be at the forefront, seeking the answers to the questions of why. My current position as an ESO Fellow allows me to continue this pursuit and continue to learn about the Universe and the technical process of its observation.

Oscar A. Gonzalez

I have been asked many times how I decided to become an astronomer, and my answer is always the same: I think life itself made that decision for me. I grew up in a small Chilean town called Chillán, and although I was always interested in science from reading magazines or books, I never really thought of it as a career path. I was good at maths and physics, and with such a profile in those years, your



Oscar A. Gonzalez

academic path was basically written in stone — studying engineering at the Universidad de Concepcion. During my last year of high school we were invited for a tour of the different departments at the University, and I decided to go and see the Physics faculty. I asked the Professor about astronomy as a career, and his answer was categorical: “You have to be a genius to do that. Only the greater minds would follow such a career.” I was discouraged and, despite my maths teacher insisting that the professor was wrong, I became an engineering student.

Life, on the other hand, seemed to have something different in mind for me. During my first year of studies, I was very sick and was forced to spend five months in bed with reduced movement. With such an experience, and having so much time on my hands to think, I decided to make a change. I would do what I wanted to do. I would try to become an astronomer at Pontificia Universidad Catolica (PUC) in Santiago.

It was very scary, moving from Chillán to an enormous city like Santiago to study something I thought I wasn't smart enough for. But once again, life gave me a helping hand. I came across a course given by Manuela Zoccali that involved trips to the observatory of the astronomy department, where we would carry out

observations, try image reduction techniques and data analysis. That was the point I realised that I was finally where I was supposed to be. I continued to work with Manuela for the duration of my studies, and she would always find a way to keep me motivated. I did my Master's thesis under her supervision, studying chemical abundances of Galactic Bulge stars, and enjoyed every minute of it.

Afterwards, it was time to think about a PhD. I wanted to keep working with Manuela, and I wanted to keep studying the Milky Way Bulge, but I had to move from Chile. During the last years of my degree I met Dante Minniti, Principal Investigator of the Vista Variables in the *Vía Láctea* (VVV) survey. This is a tremendous project to study the Bulge in a way that had never been done before, and Manuela was a member of the team. As such, she suggested I apply to the International Max Planck Research School (MPRS) PhD programme at ESO Garching to work on VVV data with Marina Rejkuba. I was lucky to be offered the position, and together we did more than I would have ever imagined. I cannot stress enough how encouraging it is to do a PhD at ESO Garching, where you are constantly surrounded by people who are passionate about science.

After my PhD, I wanted to move back to Chile to finish ongoing projects with Manuela and Dante. But above all, I wanted the chance to put my growing interest in instrumentation into practice. Applying for an ESO Fellowship in Chile was the natural thing to do to achieve this, and the decision has proven itself to be the right one time and time again. I literally get sad when I have to return from my Paranal duties... but don't tell my boss! Great interactions with colleagues and visitors have made me grow as an astronomer.

Whenever I look back, I am amazed at what I went through to get to where I am now. I went from using a little 40-centimetre telescope as a scared student at PUC, to becoming night shift coordinator for the VLT! Everybody should have the opportunity to reach their potential while doing what they are passionate about, and I will always be thankful to the people who helped me get here. Life is too short

to spend it doing something you don't love and, as someone told me recently, if you really believe in what you are doing, success is just a matter of time.

Bin Yang

Open a history book, any book — it never lacks stories about emperors, conquerors or adventurers. Rarely do we get to read stories about scientists, of whom so many devote their entire lives to trying to unlock secrets of the Universe through years of toil and yet remain almost unknown. I used to wonder what drove these people to live such lives. Recently, I think I have begun to see why.

I was attracted to science at a very young age because of my family. I was born into a teacher's family in Kunming, a sunny city in the southwest of China. Both my parents suffered through the infamous Cultural Revolution and couldn't pursue advanced degrees. On account of their unfulfilled dreams, they held a special regard for scientists and my bedtime stories were often about mathematicians or physicists. Growing up in this family, I developed a strong interest in the natural sciences. Initially, I was fascinated by insects and wanted to become an entomologist. However, at the time I was applying to universities, very few schools offered courses in entomology, and the ones that did were really about agriculture. So instead of insects, I decided to study astronomy and physics at Beijing Normal University. And this would, no doubt, be a good foundation for an academic career.

In the summer of my senior year, I got an internship to observe asteroids at the National Astronomical Observatory of China (NAOC). There I met Jin Zhu, an energetic and passionate astronomer. Using a 90-centimetre Schmidt telescope, Jin and his team discovered thousands of new asteroids and made his programme the fifth largest asteroid observation project in the world in early 2000. I didn't know much about Solar System studies, but I really enjoyed the experience of observing these mysterious asteroids that were being looked at for the first time by us! After the internship, I did some literature research and found that Solar System



Bin Yang

study is a field full of surprises and evolving fast. I joined Jin's team and finished my Masters at NAOC.

While I was considering going to the US to continue my studies, I met another important mentor in my life: David Jewitt, was a distinguished professor at the University of Hawaii (UH) at the time. Dave visited NAOC and gave a talk about recently discovered objects in the Kuiper Belt, the debris disc of the Solar System. His talk was so interesting and funny. While sitting in the audience, I wished I could work with him someday. A year later my dream came true. I was accepted to the graduate programme at UH and Dave agreed to be my dissertation advisor.

The first year in Hawaii was exciting, but also terrifying. My first-ever observing proposal, which I wrote with Karen Meech, was to observe comet 9P/Tempel 1, the target of the NASA's Deep Impact mission, using the Keck Telescope. I was overwhelmed and super stressed because *Deep Impact* seemed so much more important than anything I had worked on before. I still remember the sleepless nights I spent on that project report.

For my dissertation, I studied Jupiter's Trojan asteroids, the two swarms of small asteroids that lead and trail the planet by 60 degrees. This was observationally challenging because Jovian Trojans are small and far from the Sun and the Earth. Since I was pushing the detection limit, I was not afraid of trying new instruments or new techniques.

As a result, I ended up using all the facilities on Mauna Kea, except for the Sub-millimeter Array. Although I didn't make any ground-breaking discoveries, we were able to set upper limits on the surface water content of Jovian Trojans. The best lessons I learned from Dave are: you should never let self-doubt disturb your focus and that you should not be afraid of trying new things. Another of his mottos will always stay with me: perfection is the enemy of good enough.

After my PhD, I entered the new and expanding field of astrobiology. I was a postdoctoral fellow at NASA's Astrobiology Institute in Hawaii. Besides astronomers, my office-mates included geologists, biologists and oceanographers. Our areas of expertise were so different

and yet we were always trying to find common ground between our seemingly disparate fields. I miss the days we spent talking about amino acids, genetic codes and meteoritic chondrules.

After kissing Mauna Kea goodbye, I flew to Chile and started work on Cerro Paranal, the other great temple of telescopes. The first year I spent in Chile turned out to be a very fruitful year. Using SINFONI, we observed the famous Siding Spring comet, C/2013 A1, which made a close approach to Mars, penetrating its atmosphere in mid-October of 2014. Around the same time all the Martian rovers, spacecraft, the Hubble Space Telescope and major ground-based telescopes were focusing on this comet. Using the new extreme adaptive

optics instrument, SPHERE, my colleagues and I detected a new satellite of the multiple asteroid system, 130 Elektra. I have truly enjoyed the company of my warm-hearted ESO colleagues and fellows.

One night, I went out to look at the new laser for MUSE, propagating from Yepun. It was a clear night and the orange beam seemed to connect directly with the full Moon, as if the laser was shooting straight out from the Moon. Silver moonlight shone on the domes of the VLTs. Looking at the scene, I understood why people were willing to devote their entire lives to science and remain anonymous. Decoding the mysteries of the Universe is the ultimate reward for so many of us.

Personnel Movements

Arrivals (1 April–30 June 2015)

Europe	
Gunka, Manuela (DE)	Administrative Assistant
Gutierrez Cheetham, Pablo (CL)	Electronic Engineer
Man, Wing Shan (CN/HK)	Fellow
Meyer, Katarzyna (PL)	Budget Controller
Oberti, Sylvain (FR)	AO Physicist

Chile	
Cortes, Angela (CL)	Instrumentation Engineer

Departures (1 April–30 June 2015)

Europe	
Gojak, Domingo (DE)	Electronics Engineer
Lagos Urbina, Claudia del Pilar (CL)	Fellow
Liske, Jochen (DE)	Astronomer
Rakich, Andrew (AU)	Optical Engineer
Tobar Carrizo, Rodrigo Javier (CL)	Software Engineer
Wang, Yue (CN)	Student

Chile	
de Boer, Jozua (NL)	Student
Shultz, Matthew (CA)	Student



ESO

European Organisation
for Astronomical
Research in the
Southern Hemisphere



ESO Fellowship Programme 2015/2016

The European Organisation for Astronomical Research in the Southern Hemisphere awards several postdoctoral fellowships each year. The goal of these fellowships is to offer outstanding early-career scientists the opportunity to further develop their independent research programmes in the exciting scientific environment of one of the world's foremost observatories.

ESO is the foremost intergovernmental astronomy organisation in Europe. Its approximately 110 staff astronomers, 40 Fellows and 50 PhD students conduct frontline research in fields ranging from exoplanets to cosmology, offering one of the most vibrant and stimulating scientific settings anywhere in the world.

Fellowships are available both at ESO's Headquarters in Garching near Munich, Germany, and at ESO's astronomy centre in Santiago, Chile.

ESO Headquarters is situated in one of the most active research centres in Europe, boasting one of the highest concentrations of astronomers. ESO's offices are adjacent to the Max Planck Institutes for Astrophysics and for Extraterrestrial Physics and close to the Observatory of Munich's Ludwig-Maximilian University. Additionally, ESO participates in the Excellence Cluster Universe at the Garching campus, which brings together nearly 200 scientists to explore the origin and structure of the Universe. Consequently, ESO Fellows in Garching have many opportunities to interact and collaborate with astronomers at neighbouring institutes.

In Chile, fellows have the opportunity to collaborate with the rapidly growing Chilean astronomical community as well as with astronomers at other international observatories located in Chile. The advent of the new ALMA building next to ESO's Santiago offices and the arrival of many astronomers and fellows working on the ALMA project have further enhanced the stimulating scientific environment available to ESO Chile Fellows.

The fellowships in Garching start with an initial contract of one year followed by a two-year extension (three years total). In addition to developing their independent research programmes, ESO Garching Fellows will be expected to engage in some functional work, for up to 25% of their time, related to, e.g., instrumentation, the VLT, ALMA, E-ELT, science operations support either in Garching or at one of ESO's observatories in Chile, or public outreach. This provides the fellows with the opportunity to get involved with ESO projects or operations, and to gather valuable insights and experience not available in any other setting.

The fellowships in Chile are granted for one year initially, with annual extensions for three additional years (four years total). During the first three years, the fellows are assigned to one of the science operations groups of Paranal, ALMA or APEX, where they will contribute to the operations at a level of 80 nights per year. For ALMA fellows, a fraction of their duties can alternatively be spent on data processing, participation in the ALMA review process as technical experts, software testing, and optimisation and extension of the array capabilities.

During the fourth year of Chile fellowships several options are provided. The fellow may be hosted by a Chilean institution where she/he will be eligible to apply for time on all telescopes in Chile through competition for Chilean observing time. Alternatively, the fellow may choose to spend the fourth year either at ESO's astronomy centre in Santiago, at ESO Headquarters in Garching or at any astronomy/astrophysics institute in an ESO Member State. There are no functional duties during the fourth year, except in the case that the fourth year is spent at ESO Chile where fellows are expected to carry out functional work for up to 25% of their time.

The programme is open to applicants who will have achieved their PhD in astronomy, physics or a related discipline before 1 November 2016. Early-career scientists from all astrophysical fields are welcome to apply. Scientific excellence is the primary selection criterion for all fellowships.

We offer an attractive remuneration package including a competitive salary and allowances (tax-free), comprehensive social benefits, and we provide financial support for relocating families.

If you are interested in enhancing your early career through an ESO Fellowship, then please apply by completing the web application form available at <http://jobs.eso.org>.

Please include the following documents in your application:

- a cover letter;
- a curriculum vitae with a list of publications;
- a proposed research plan (maximum of two pages);
- a brief outline of your technical/observational experience (maximum of one page);
- the names and contact details of three persons familiar with your scientific work and willing to provide a recommendation letter. Referees will be automatically invited to submit a recommendation letter. However, applicants are strongly advised to trigger these invitations (using the web application form) well in advance of the application deadline.

The closing date for applications is 15 October 2015. Review of the application documents, including the recommendation letters, will begin immediately. Incomplete or late applications will not be considered.

Candidates will be notified of the results of the selection process between December 2015 and February 2016. Fellowships will begin in the second half of 2016.

Further information

For more information about the fellowship programme and ESO's astronomical research activities, please see: <http://www.eso.org/sci/activities/FeSt-overview/ESOfellowship.html>.

For a list of current ESO Staff and Fellows, and their research interests please see: <http://www.eso.org/sci/activities/personnel.html>.

Details of the Terms of Service for fellows including details of remuneration are available at: <http://www.eso.org/public/employment/fellows.html>.

For any additional questions please contact:

For Garching: Eric Emsellem, Tel. +49 89 3200 6914,
email: eric.emsellem@eso.org.

For Chile: Claudio De Figueiredo Melo, Tel. +56 2 463 3032,
email: cmelo@eso.org.

Although recruitment preference will be given to nationals of ESO Member States (members are: Austria, Belgium, Brazil, the Czech Republic, Denmark, Finland, France, Germany, Italy, the Netherlands, Poland, Portugal, Spain, Sweden, Switzerland and United Kingdom), no nationality is in principle excluded.

The post is equally open to suitably qualified female and male applicants.





The two mountains of ESO's Observatory in the Atacama Desert, in reality separated by 28 kilometres. Right: The Very Large Telescope on Cerro Paranal, which has been in operation since 1999. Left: Preparation work for the site of the European Extremely Large Telescope on Cerro Armazones. The road, under construction, will join the two observing sites.



ESO, the European Southern Observatory, is the foremost intergovernmental astronomy organisation in Europe. It is supported by 16 countries: Austria, Belgium, Brazil, the Czech Republic, Denmark, France, Finland, Germany, Italy, the Netherlands, Poland, Portugal, Spain, Sweden, Switzerland and the United Kingdom. ESO's programme is focused on the design, construction and operation of powerful ground-based observing facilities. ESO operates three observatories in Chile: at La Silla, at Paranal, site of the Very Large Telescope, and at Llano de Chajnantor. ESO is the European partner in the Atacama Large Millimeter/submillimeter Array (ALMA). Currently ESO is engaged in the design of the European Extremely Large Telescope.

The Messenger is published, in hard-copy and electronic form, four times a year: in March, June, September and December. ESO produces and distributes a wide variety of media connected to its activities. For further information, including postal subscription to The Messenger, contact the ESO education and Public Outreach Department at:

ESO Headquarters
Karl-Schwarzschild-Straße 2
85748 Garching bei München, Germany
Phone +49 89 320 06-0
information@eso.org

The Messenger:
Editor: Jeremy R. Walsh;
Design, Production: Jutta Boxheimer;
Layout, Typesetting: Mafalda Martins;
Graphics: Kerstin Bauer.
www.eso.org/messenger/

Printed by Color Gruppe
Geretsrieder Straße 10
81379 München, Germany

Unless otherwise indicated, all images in The Messenger are courtesy of ESO, except authored contributions which are courtesy of the respective authors.

© ESO 2015
ISSN 0722-6691

Contents

Telescopes and Instrumentation

Vlahakis C. et al. – ALMA Extends to 15-kilometre Baselines: Submillimetre Science down to 20-Milliarcsecond Resolution	2
---	---

Astronomical Science

Maercker M. et al. – Probing the Effects of Stellar Evolution: The Dust and Gas in Detached Shells around AGB Stars	9
Gullieuszik M. et al. – OmegaWINGS: A VST Survey of Nearby Galaxy Clusters	13
Smith R. J. et al. – The SINFONI Nearby Elliptical Lens Locator Survey (SNELLS)	18
Zafar T. et al. – The ESO UVES Advanced Data Products Quasar Sample: Neutral Gas Mass and Metal Abundances in the Universe	23

Astronomical News

Rejkuba M. et al. – Report on the ESO Workshop “Baryons at Low Densities: The Stellar Halos around Galaxies”	28
Vlahakis C. – Report on the ESO Workshop “Dissecting Galaxies Near and Far”	31
Hatziminaoglou E. et al. – Report on the “ALMA/Herschel Archival Workshop”	35
Fellows at ESO – J. Anderson, O. A. Gonzalez, B. Yang	37
Personnel Movements	40
ESO Fellowship Programme 2015/2016	41

Front cover: A collage of images of the Atacama Large Millimeter/submillimeter Array (ALMA) and some scientific results, prominently featuring images from the Long Baseline Campaign. ALMA images of the gravitationally lensed submillimetre galaxy SDP.81, the dust disc around the young star HL Tauri, the resolved dust shell of the late-type binary star Mira B and the asteroid Juno are displayed; see the article on the Long Baseline Campaign by Vlahakis et al. (p. 2) for details. The other images, from ALMA Early Science releases, are of the ring around the young star Fomalhaut, the spiral outflow around R Sculptoris, the Antennae Galaxies (NGC 4038 and NGC 4039) and SN 1987A.

Credits: ESO; ALMA (NRAO/ESO/NAOJ); NASA/ESA Hubble Space Telescope; Y. Tamura; A. Angelich (NRAO/AUI/NSF); NASA Chandra Space Telescope; A. Russell; C. Malin; B. Tafreshi (twanight.org); A. Duro; M. Maercker et al.; C. Vlahakis et al.; W. Vlemmings et al.

